A Mathematical Model of the Iron Regulatory Network in *Aspergillus Fumigatus*

Madison Brandon

Dissertation submitted to the Faculty of the
Virginia Polytechnic Institute and State University
in partial fulfillment of the requirements for the degree of

Masters of Science
in
Mathematics

Reinhard Laubenbacher, Chair
Christopher Lawrence
Stanca Cuipe

25 April 2013
Blacksburg, Virginia

Keywords: *Aspergillus fumigatus*, discrete model, iron regulation, siderophores, gene regulatory network, genetic oscillations, qRT-PCR

A Mathematical Model of the Iron Regulatory Network in *Aspergillus Fumigatus*

Madison Brandon

(ABSTRACT)

Aspergillus fumigatus is an opportunistic fungal pathogen responsible for invasive aspergillosis in immunocompromised individuals. Current detection and treatment strategies for invasive aspergillosis, as well as other invasive fungal infections, are poor. Iron has been shown to be essential for *Aspergillus fumigatus* virulence. Furthermore, mechanisms in the iron regulatory network are believed to be potential drug targets since iron management in fungi is vastly different from that in mammals and other eukaryotes. Therefore a better understanding of iron homeostasis in *Aspergillus fumigatus* could help improve drug therapies for invasive aspergillosis. In this research a discrete model of iron uptake, storage and utilization in *Aspergillus fumigatus* with particular focus on siderophore-mediated iron acquisition is constructed. The model predicts oscillations in gene expression as the fungus adapts to a switch from an iron depleted to an iron replete environment. The model is validated via *in vitro* experiments.

Acknowledgments

I would like to thank my committee members Dr. Reinhard Laubenbacher, Dr. Chris Lawrence, and Dr. Stanca Ciupe. I especially thank: my advisor, Dr. Reinhard Laubenbacher, for all his advice, support, and feedback, Dr. Chris Lawrence for allowing me access to his lab, and Brad Howard for patiently teaching me all required lab techniques.

I would also like to thank my research group: Matt Oremland, Shernita Lee, Claus Kadelka, Seda Arat, Cory Brunson, Anael Verdugo, Katarzyna Swirydowicz, Jennifer Galovich, and Kathy O'Hara. Without their feedback and collaboration this project would not have been possible. In particular, thank-you to Shernita and Seda for first helping me to understand how to build a discrete model. Thank-you to Aneal for providing valuable tips and advise about giving good presentations. And thank-you to Jennifer and Kathy for proofreading so many of my various papers.

Finally, I would like to give a special thanks to Betsy Williams for being the best team mom a research group could ask for.

Contents

List of Tables

List of Figures

Chapter 1

Introduction

Aspergillus fumigatus is a ubiquitous, saprophytic fungus which has become an increasingly dangerous fungal pathogen of humans worldwide. In particular, *A. fumigatus* is responsible for invasive aspergillosis (IA), a major cause of mortality in immunocompromised human hosts. The population of immunocompromised individuals is growing and includes patients with haematological malignancies such as leukemia, cancer patients receiving cytotoxic chemotherapy, solid-organ and hematopoietic stem-cell transplant patients, patients on prolonged corticosteroid therapy, patients with genetic immunodeficiencies, and HIV/AIDS patients [32] [11]. A 2001 literature review established a case-fatality rate (CFR) of 58% for invasive aspergillosis in studies reported after 1995 [33]. Prevention, detection, and treatment strategies for IA remain poor despite thorough study [34].

One of the major challenges to treating invasive fungal infections is that fungi and mammals are both eukaryotes and hence have very similar molecular composition and functioning. This makes it difficult to design drugs which target the fungus yet at the same time do not harm the human host. The focus on iron metabolism is motivated by the fact that iron homeostasis mechanisms in fungi are substantially different from those in other eukaryotes [35]. Since the development of antifungals hinges on the ability to exploit differences in molecular functioning between the fungus and host, this difference in iron-handling makes the iron regulatory network a potential target for therapeutic intervention [2]. In particular, fungi possess a unique iron acquisition system in which iron is sequestered from host proteins via siderophores, low-molecular-mass iron chelating compounds secreted by the fungus. Notably, a mutant *A. fumigatus* strain unable to produce siderophores was avirulent in a mouse model of IA [11]. Furthermore, iron deprivation of invading pathogens by the host is the first line of host defense [37]. Therefore, iron is an important virulence factor.

Iron is an essential nutrient for all eukaryotes. Both the fungus and host require iron for important cellular functions including respiration, oxidative stress, gene regulation, and DNA synthesis [36]. Conversely, iron is toxic in excess as it can cause the formation of reactive oxygen species (ROS). Thus tight regulatory mechanisms are required to maintain iron homeostasis and to quickly adapt to changing iron levels in the environment. In contrast to mammals, iron excretory mechanisms have not yet been identified in fungi [13]. Hence control of iron uptake is believed to be the major iron homeostasis mechanism in *A. fumigatus*. For this reason the model presented here places particular emphasis on iron uptake systems, especially siderophore-mediated iron uptake.

In order to make improvements in the treatment of invasive fungal infections like invasive aspergillosis, a more complete understanding of the fungal iron regulatory network is crucial. For this

purpose, I have constructed a novel dynamic mathematical model of iron acquisition, storage, and utilization in *A. fumigatus*. Mathematical modeling has become an indispensable tool in systems biology research. A fundamental problem in biology is to describe and understand how complex molecular interaction networks operate. Mathematical modeling of these systems allows the encoding of dynamic interactions among molecules which informs our understanding of molecular functioning. Dynamic computational models can offer insights into underlying mechanisms and can be used to predict novel gene functions and interactions, which can then be tested in the lab. In this respect, one can think of models as virtual laboratories to generate and test hypothesis. Recently a first step in the direction of modeling iron homeostasis, model inference from high-throughput data, in *A. fumigatus* was made by one of the leading research groups in this field [15]. However, to my knowledge a dynamic mathematical model does not yet exist. The methodology here follows a systems biology approach of modeling procedures followed by experimental validation of model predictions. The ultimate goal is not to design drugs for IA but to gain a deeper understanding of iron homeostasis in *A. fumigatus* and discover novel mechanisms in the iron regulatory network.

The goals of this research are:

1. Build a model of the iron regulatory network in *A. fumigatus* with particular emphasis on siderophore-mediated iron acquisition.
2. Explore long term dynamics of the model both within a deterministic and stochastic framework.
3. Validate experimentally the model prediction of oscillatory steady state behavior in iron replete environments.
4. Offer biological hypotheses as to why this oscillatory behavior is observed is this system.

In the following chapters I first give mathematical background on discrete dynamical systems modeling frameworks. Second, I describe all genes, proteins and enzymes in the *A. fumigatus* iron regulatory system that are modeled. Third, I describe the mathematical model and give a brief example of model construction. Fourth, I present results from steady state and knockout analysis of the deterministic model that are supported by current literature. I then introduce a novel model prediction, oscillatory steady state behavior in an iron replete environment, and analyze this behavior in a stochastic framework. Next I show how the model prediction is validated via real-time, quantitative reverse transcriptase polymerase chain reaction (qRT-PCR) experiments and detail all experimental methods. Finally I conclude with a discussion of what we may infer about genetic oscillations in *A. fumigatus* iron regulation. The computational tools used for model analysis are freely available through our web-based software ADAM, http://dvd.vbi.vt.edu/adam.html.

Chapter 2

Mathematical Background

The model presented in this paper is a discrete model. Discrete models are time- and state-discrete dynamical systems in which variables can take on only a finite number of states and variable interactions are described by logical rules. Several different discrete model types have established communities in the biological sciences, including probabilistic Boolean networks, logical models, bounded petri-nets, and agent-based models. Discrete modeling approaches have been applied to a wide variety of biological contexts including metabolic networks, gene regulatory networks and signal transduction networks [22]. These models are built from qualitative information and provide an intuitive picture of a network. My choice to use a discrete model as opposed to a continuous model was motivated by the fact that continuous models, such as ordinary or partial differential equation models, rely on quantitative information such as kinetic rate constants for biochemical reactions or diffusion parameters. Since little quantitative information in terms of kinetic parameters is known about fungal iron regulation, discrete modeling provides a fitting alternative framework to capture the dynamics of this system. Furthermore, interaction mechanisms of regulatory networks like the iron regulatory network in *A. fumigatus* are well described by logical statements that are characteristic of discrete models.

In the following sections I will introduce the three discrete modeling frameworks I used to model iron homeostasis in *A. fumigatus*: discrete dynamical systems, polynomial dynamical systems, and stochastic dynamical systems.

2.1 Discrete Dynamical Systems

Definition 2.1. *Let $x_1, ..., x_n$ be variables which can take values in finite sets $X_1, ..., X_n$ respectively, and let $X = X_1 \times \cdots \times X_n$ be the Cartesian product. A* ***discrete dynamical system*** *is a function*

$$f = (f_1, ..., f_n) : X \to X$$

where the update rules or coordinate functions of variable x_i are $f_i : X \to X_i$ for $i = 1, ..., n$.

Definition 2.2. *Let $f = (f_1, ..., f_n) : X \to X$ be a discrete dynamical system in n variables, $x_1, ..., x_n$, as defined above in Definition 2.1. Then, $\bar{x} = (x_1, ..., x_n)$ is called a* ***state*** *of the system.*

Consider the following two-node boolean example of a discrete dynamical system. This system could represent the interaction between two proteins in which each protein can reside in one of two states: 0 or 1. Biologically, state 0 could represent inactive, low concentration, not phosphorylated,

etc. depending on what the node is and how it interacts with other nodes in the system. Similarly, 1 might represent active, high concentration, phosphorylated, etc.

Example 2.3. *Let $n = 2$ and $X = \{0, 1\} \times \{0, 1\}$. Consider the discrete dynamical system*

$$f = (f_1, f_2) : X \to X$$

where mappings f_1 and f_2, defining how variables x_1 and x_2, respectively, are updated at each time step respectively, are given by the following logical rules:

$$f_1(\bar{x}) = \begin{cases} 0, & x_1 = 0 \\ 1, & x_1 = 1 \end{cases}$$

$$f_2(\bar{x}) = \begin{cases} 0, & x_1 = x_2 = 1 \\ 1, & x_1 = 0 \text{ or } x_2 = 0 \end{cases}$$

It is convenient to encode this information in transition tables or truth tables. These are tables in which all possible input configurations to update rules, f_1 and f_2, at time t are listed in the left-hand side of the table, and the outputs at time $t + 1$ are listed in the right most column of the table. Transition tables for x_1 and x_2 are Tables 2.1 and 2.2, respectively. Note that x_1 takes only itself as an input while x_2 takes both itself and x_1 as inputs. The wiring diagram in Figure 2.1 is a static representation of the system showing which variables are influenced by which other variables.

$x_1(t)$	$x_1(t+1)$
0	0
1	1

Table 2.1: Transition table for variable x_1 in Example 2.3.

$x_1(t)$	$x_2(t)$	$x_2(t+1)$
0	0	1
0	1	1
1	0	1
1	1	0

Table 2.2: Transition table for variable x_2 in Example 2.3.

Once the wiring diagram and all transition tables are specified, an update schedule must be decided on. An update schedule is merely the order in which the rules in the transition tables are applied. For most of the model analysis in this paper, a deterministic model with synchronous

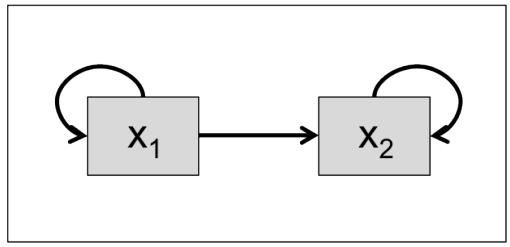

Figure 2.1: Wiring Diagram in Example 2.3.

update schedule has been assume. This means that all nodes or proteins in the network are updated at the same time, i.e. all rules are applied at once. The nodes can also be updated sequentially, i.e. in some fixed order, or asynchronously, i.e. randomly.

Upon experiencing some environmental perturbation, a biological system will eventually reach a resting state or an oscillation. In modeling terms, these attracting states correspond to states in the model which, after applying an update, the model remains in the same state or cycles infinitely through a set of states. When the model remains in the same state this state is called a steady state or fixed point. When the model cycles infinitely through a set of states these states are collectively called a limit cycle.

Definition 2.4. *Let $\bar{x} = (x_1, ..., x_n)$ be a state in the discrete dynamical system $f = (f_1, ..., f_n)$. $\bar{x}$ is called a* ***steady state*** *(or fixed point) of the system if $f(\bar{x}) = \bar{x}$.*

Definition 2.5. *A state $\bar{x} = (x_1, ..., x_n)$ has period m if $f(\bar{x})^m = \bar{x}$ and $f(\bar{x})^j \neq \bar{x}$ for all $1 \leq j < m$.*

Definition 2.6. *Let $\bar{x}_1 = (x_{1_1}, ..., x_{1_n}), \bar{x}_2 = (x_{2_1}, ...x_{2_n}), ..., \bar{x}_m = (x_{m_1}, ..., x_{m_n})$ be a set of m states in the discrete dynamical system $f = (f_1, ..., f_n)$. $(\bar{x}_1, ..., \bar{x}_m)$ is called a* ***limit cycle*** *(or m-cycle) of the system if $f(\bar{x}_1) = \bar{x}_2, f^2(\bar{x}_1) = \bar{x}_3$,...,$f^{m-1}(\bar{x}_1) = \bar{x}_m$ and $\bar{x}_i$ has period m for all $i = 1, ..., m$.*

After an update schedule has been decided on, equilibrium solutions can be found by enumerating or simulating the entire state space. Note that in an ordinary differential equation system a steady state is only reached at $t = \infty$, unless the model is initialized at that steady state. However in discrete models, a steady state can be reached in a finite number of steps.

Example 2.7. *Recall the discrete dynamical system in Example 2.3 in which $n = 2$ and $X = \{0, 1\} \times \{0, 1\}$. This example model is very small, so one can easily chart all possible trajectories by writing out where each state in the network moves to at the next time step. This information is displayed in a graph called the state space, see Figure 2.2.*

Looking at the state space, one can easily pick out dynamic features such as steady states and limit cycles. The arrow looping from state $(0, 1)$ back to itself means that once the state $(0, 1)$ is reached the model will never leave that state. Thus $(0, 1)$ is a steady state. There is also a limit cycle in which the model repeatedly visits states $(1, 0)$ and $(1, 1)$. Note that there are two components in the state space graph. In modeling terminology these components are called basins of attraction. One basin of attraction leads to the steady state $(0, 1)$. The other basin of attraction is the 2-cycle $\{(1, 0), (1, 1)\}$. Another helpful way to display model dynamics is through a trajectory plot. In this

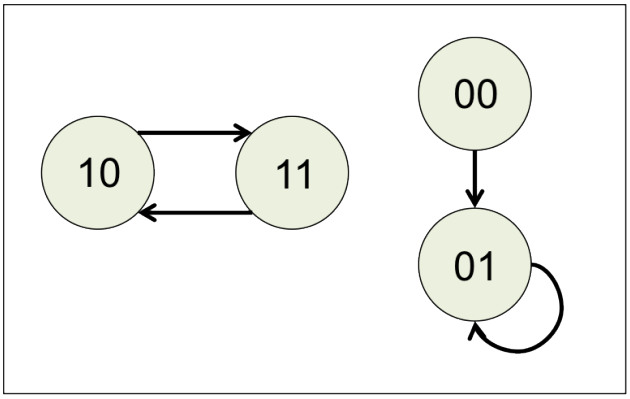

Figure 2.2: State Space for discrete dynamical system in Example 2.3.

type of plot the model is initialized to some state and a trajectory of one or more variables is plotted as a function of time. Figures 2.3a and 2.3b show two sample trajectories, each initialized in one of the two basins of attraction.

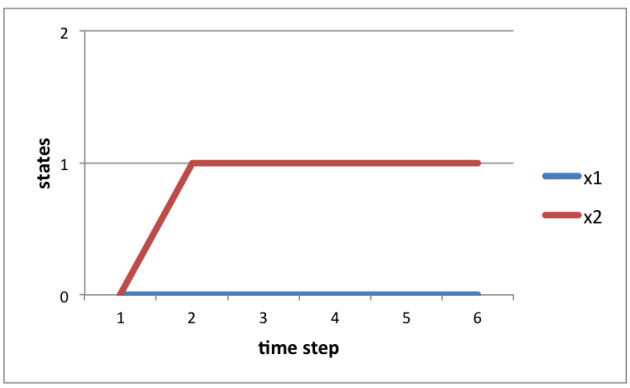

(a) Sample trajectory of the discrete dynamical system presented in Example 2.3. For this trajectory the model was initialized at state $(0, 0)$, i.e. from within the basin of attraction containing the fixed point.

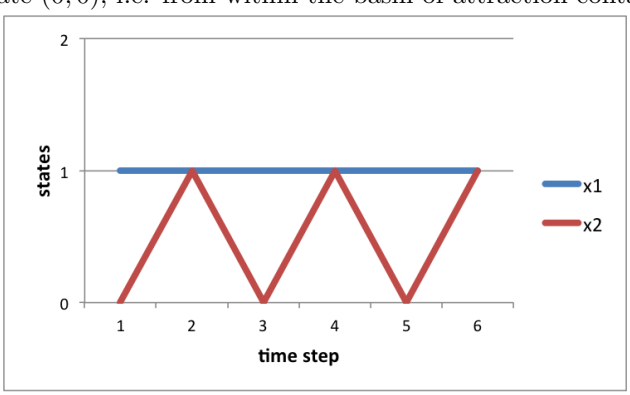

(b) Sample trajectory of the discrete dynamical system presented in Example 2.3. For this trajectory the model was initialized at state $(1, 0)$, i.e. from within the basin of attraction containing the 2-cycle.

Figure 2.3: Trajectories from two different initial states of the model in Example 2.3.

2.2 Polynomial Dynamical Systems

For analysis purposes discrete models may be represented as mathematical objects within the framework of polynomial dynamical systems (PDS), a system of polynomial equations over a finite field.

Definition 2.8. *(Laubenbacher* et. al. *[24]) Let p be a prime and let $f_1, ..., f_n \in \mathbb{F}_p[x_1, ...x_n]$ be polynomials. A* ***polynomial dynamical system*** *(PDS) F over the finite field $\mathbb{F}_p$ is a function*

$$F = (f_1, ..., f_n) : \mathbb{F}_p^n \to \mathbb{F}_p^n$$

The polynomials $f_1, ..., f_n$ are the coordinate functions of variables $x_1, ..., x_n$ with $f_i : \mathbb{F}_p^n \to \mathbb{F}_p$ for $i = 1, ..., n$. Iteration of F results in a time-discrete dynamical system.

It has been shown that any function in n variables over a finite field of prime characteristic p can be uniquely expressed by a polynomial of degree at most $n(p-1)$.[23]

Theorem 2.9. *(Lidl* et. al. *[23]) Let k be a finite field, and $f : k^r \to k$ be any function. Then there exists a unique minimal degree polynomial $g : k^r \to k$ such that $f(x) = g(x)$ for all $x \in k^r$.*

Thus each transition table can be uniquely encoded in a polynomial using Lagrange interpolation [22]:

$$g(\bar{x}) = \sum_{(c_{i_1}, ..., c_{i_r}) \in k^r} f(c_{i_1}, ..., c_{i_r}) \prod_{j=1}^{r} (1 - (x_j - c_{ij})^{p-1}) \pmod p$$

where $c_{i_1}, ..., c_{i_r}$ are the values of the r variables $x_{i_1}, ..., x_{i_r}$ which are inputs to variable x_i at time t, i.e. the left-hand side of the transition table for x_i. And $f(c_{i_1}, ..., c_{i_r})$ is the output at time $t+1$ for the input configuration $c_{i_1}, ..., c_{i_r}$, i.e. the right-hand side of the transition table. For our purposes, $k = \mathbb{F}_p = \{0, 1, ..., p-1\}$ where p is the maximum prime number of the different discrete values that all variables can take.

Example 2.10. *Again consider the discrete dynamical system from Example 2.3. Polynomial functions encoding the update rules of each variable can be obtained by interpolating the transition tables, Tables 2.1 and 2.2, using the formula above. First note that the maximum number of states is two; therefore, $p = 2$ and $k = \mathbb{F}_2$. The transition table for x_1 is Table 2.1, so x_1 is the only input variable to x_1. Hence $r = 1$ and the mapping f_1 is defined on $\mathbb{F}_2 = \{0, 1\}$ as follows:*

$$f_1(0) = 0$$
$$f_1(1) = 1$$

The polynomial update function g_1 that defines the same mapping as f_1 for x_1 is constructed as follows:

$$\begin{aligned} g_1(\bar{x}) &= \sum_{(c_1) \in \mathbb{F}_2} f_1(c_1) \prod_{j \in \{1\}} (1 - (x_j - c_j)^{2-1}) \pmod 2 \\ &= f_1(0) \cdot (1 - (x_1 - 0)) + f_1(1) \cdot (1 - (x_1 - 1)) \pmod 2 \\ &= 0 + 1 - (x_1 - 1) \pmod 2 \\ &= 2 - x_1 \pmod 2 \\ &= x_1 \end{aligned}$$

The transition table for x_2 is Table 2.2 which shows that both x_1 and x_2 are inputs to x_2. Hence $r = 2$ for x_2 and the mapping f_2 is defined on $\mathbb{F}_2^2 = \{0,1\} \times \{0,1\}$ as follows:

$$\begin{aligned} f_2(0,0) &= 1 \\ f_2(0,1) &= 1 \\ f_2(1,0) &= 1 \\ f_2(1,1) &= 0 \end{aligned}$$

The polynomial update function g_2 that defines the same mapping as f_2 for x_2 is constructed as follows:

$$\begin{aligned} g_2(\bar{x}) = & \sum_{(c_1,c_2)\in\mathbb{F}_2^2} f_2(c_1,c_2) \prod_{j\in\{1,2\}} (1-(x_j-c_j)^{2-1}) \pmod 2 \\ =& f_2(0,0)\cdot(1-(x_1-0))\cdot(1-(x_2-0))+ \\ & f_2(0,1)\cdot(1-(x_1-0))\cdot(1-(x_2-1))+ \\ & f_2(1,0)\cdot(1-(x_1-1))\cdot(1-(x_2-0))+ \\ & f_2(1,1)\cdot(1-(x_1-1))\cdot(1-(x_2-1)) \pmod 2 \\ =& 1\cdot(1-(x_1-0))\cdot(1-(x_2-0))) + 1\cdot(1-(x_1-0))\cdot(1-(x_2-1))+ \\ & 1\cdot(1-(x_1-1))\cdot(1-(x_2-0)) + 0\cdot(1-(x_1-1))\cdot(1-(x_2-1)) \pmod 2 \\ =& (1+x_1)\cdot(1+x_2) + (1+x_1)\cdot(x_2) + x_1\cdot(1+x_2) \pmod 2 \\ =& 1 + x_2 + x_1 + x_1x_2 + x_2 + x_1x_2 + x_1 + x_1x_2 \pmod 2 \\ =& 1 + x_1x_2 \end{aligned}$$

The polynomials calculated in Example 2.10 agree with the update rules found by inspecting the tables. Finding the update functions simply by looking at the transition tables is only possible when the model is very small. Furthermore, as a model becomes increasing complex it becomes impossible to analyze by computer simulation alone. For instance, a boolean model with 30 nodes already has 2^{30} or over 1 billion states. By translating these models into algebraic objects, computational tools, rather than brute force enumeration, can be used to solve for interesting dynamics. Once a discrete model has been converted from transition tables to PDS form one can apply methods and theory from abstract algebra and algebraic geometry to look for steady states and limit cycles. Attracting solutions can be obtained from a PDS by solving the following polynomial systems:
For fixed points:

$$\begin{aligned} f_1(\bar{x}) &= x_1 \\ &\vdots \\ f_n(\bar{x}) &= x_n \end{aligned}$$

For limit cycles of length m:

$$\begin{aligned} f_1^m(\bar{x}) &= x_1 \\ &\vdots \\ f_n^m(\bar{x}) &= x_n \end{aligned}$$

Example 2.11. *Fixed points for the PDS in Example 2.10 can be calculated by solving the system*

$$f_1(\bar{x}) = x_1 = x_1$$
$$f_2(\bar{x}) = 1 + x_1x_2 = x_2$$

It is simple to check that $(0, 1)$ *is the only state that satisfies the above system. Likewise, one can check for* 2*-cycles by solving*

$$f_1^2(\bar{x}) = x_1 = x_1$$
$$f_2^2(\bar{x}) = 1 + x_1(1 + x_1x_2) = x_2$$

Again, one can check that $(1, 0)$, $(1, 1)$, and $(0, 1)$ are the only states satisfying these equations. However, $(0, 1)$ is already a steady state, i.e. a solution of period 1, and hence it cannot also be a 2-cycle. States $(1, 0)$ and $(1, 1)$ are not already steady states , so they do in fact have period 2 and are part of a 2-cycle.

It is not difficult to imagine how complicated these polynomials can become as the system grows large. The polynomials in general will be highly non-linear. One computational tool that is extremely helpful in solving these types of systems is Gröbner bases. Analysis of Dynamic Algebraic Models (ADAM), a free web-based software tool which analyzes the dynamics of discrete models using Gröbner bases, is available at http://dvd.vbi.vt.edu/adam.html. For more details on the software package and how these computations are implemented see Hinkelmann *et. al.* [25] The model presented in this paper is analyzed via a combination of computational algebra and simulation.

2.3 Stochastic Discrete Dynamical Systems

The modeling framework described above are deterministic. However, many biological processes exhibit a high degree of stochasticity [38] [39] [40] [41]. For instance, Elowitz *et al.* show that the amount of protein produced by a particular gene can vary from cell to cell due to sources of extrinsic and intrinsic noise [38]. In order to introduce stochasticity into the model the stochastic discrete dynamical systems (SDDS) framework was employed. A stochastic discrete dynamical system is a time- and state-discrete dynamical system modeling stochasticity at the functional level.

Definition 2.12. *(Murrugarra* et. al. *[30]) Let* $x_1, ..., x_n$ *be variables which can take values in finite sets* $X_1, ..., X_n$ *respectively. Let* $X = X_1 \times \cdots \times X_n$ *be the Cartesian product, and* $f_i : X \to X_i$ *be the update function for* x_i *for all* $i = 1, ..., n$*. Let* $p_i^{\uparrow}$ *be the probability that variable* x_i *will be updated given that* f_i *specifies an increase in state at the next time step. Let* $p_i^{\downarrow}$ *be the probability* x_i *will be updated given that* f_i *specifies a decrease in state at the next time step. A* ***stochastic discrete dynamical system*** *is a collection of triplets*

$$\{f_i, p_i^{\uparrow}, p_i^{\downarrow}\}_{i=1}^{n}.$$

The probabilities $p_i^{\uparrow}, p_i^{\downarrow} \in [0,1]$ for all $i \in \{1, ..., n\}$ and are called the activation propensity and degradation propensity, respectively, of the i-th variable in the system. The stochasticity in this framework is introduced via these propensity parameters. The activation propensity indicates how likely the value of x_i is to be increased in cases where the update rule dictates an increase in state at the next time step. Hence $1-p_i^{\uparrow}$ indicates how likely the value of x_i is to remain in the same state in cases where the update rule dictates an increase in state at the next time step. On the other hand, the degradation propensity indicates how likely the value of x_i is to be decreased in cases where the update rule dictates a decrease in state at the next time step. And $1 - p_i^{\downarrow}$ indicates how likely the value of x_i is to remain in the same state in cases where the update rule dictates a decrease in state at the next time step. If the update rule of x_i dictates that x_i remain in the same state at the next time point, then neither $p_i^{\uparrow}$ nor $p_i^{\downarrow}$ apply and x_i remains in its current state with probability 1. Therefore, steady states are preserved regardless of whether the deterministic or stochastic framework is applied. Note that $p_i^{\uparrow}$ and $p_i^{\downarrow}$ are independent probabilities and are not required to sum to 1.

The propensities are analogous to activation and degradation kinetic rates in differential equations modeling. If $p_i^{\uparrow} = p_i^{\downarrow} = 0.5$ for all $i = 1, .., n$ then each variable at each time step is equally likely to be either updated (activated or degraded) according to its update rule or remain in its current state. If $p_i^{\uparrow} = p_i^{\downarrow} = 1$ for all $i = 1, ..., n$ then each variable will be updated according to its update function with probability 1, i.e. the system becomes deterministic. Stochastic discrete dynamical systems (SDDS) can also be represented as polynomial dynamical systems with propensity parameters.

Example 2.13. *The discrete dynamical system from Example 2.3 is deterministic with synchronous updating. Now consider this system within the SDDS framework with a uniform random update schedule, i.e.* $p_i^{\uparrow} = p_i^{\downarrow} = 0.5$ *for all* $i = 1, .., n$. *The propensity matrix is shown in Table 7.1.*

	$p^{\uparrow}$	$p^{\downarrow}$
x_1	0.5	0.5
x_2	0.5	0.5

Table 2.3: Propensity matrix to incorporate stochasticity into Example 2.3.

The SDDS in variables x_1 *and* x_2 *is*

$$(\{f_1, 0.5, 0.5\}, \{f_2, 0.5, 0.5\})$$

where $f_1 = x_1$ *and* $f_2 = 1 + x_1x_2$ *as in Example 2.10.*

The static representation or wiring diagram (Figure 2.1) for the SDDS is the same as in the deterministic case. However the transition between states may be slightly different due to propensity. See Figure 2.4 to see how the state space of Example 2.3 is altered when a uniformly distributed random update schedule is applied.

More interesting than the state space is a trajectory plot of the SDDS. Now that the model is no longer deterministic it is interesting to view the averaged trajectories of many stochastic simulations. Figure 2.5 shows an average of 100 stochastic trajectories of the SDDS in Example 2.13 with

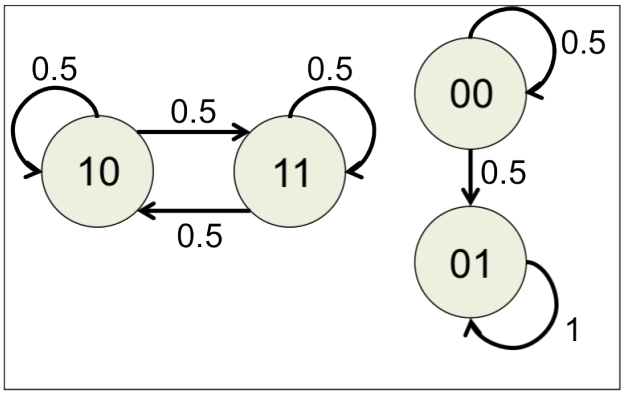

Figure 2.4: State Space for the SDDS with random update schedule in Example 2.13.

a uniformly distributed random update schedule over 50 time steps. Each trajectory is initialized from the same state within the basin of attraction consisting of the 2-cycle. Note how the trajectory plot of the SDDS differs from that of the deterministic model, Figure 2.3b.

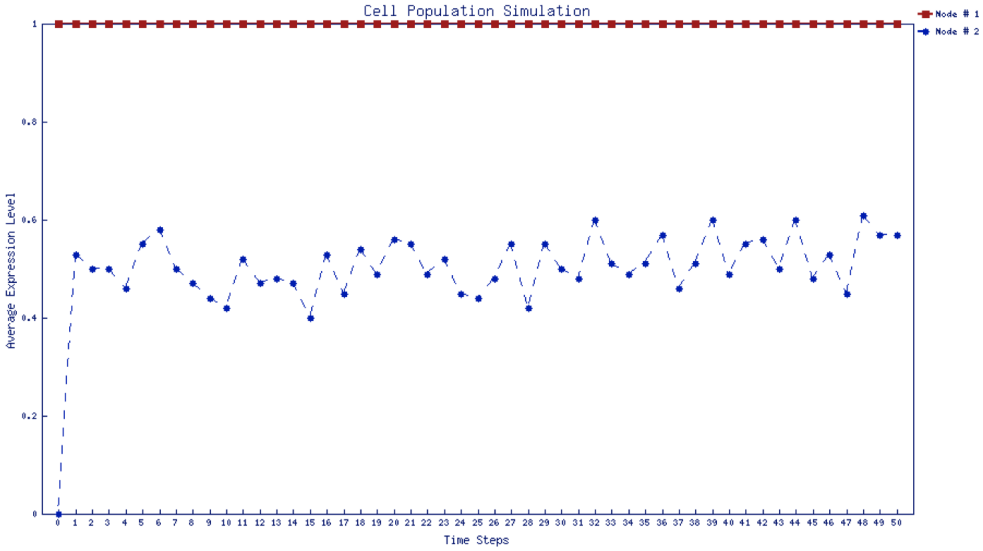

Figure 2.5: Sample trajectory of 100 individuals of the SDDS in Example 2.13.

This small example indicates how different update schedules can affect the dynamics of a network.

Chapter 3

Biological Background

In order to avoid iron toxicity and adapt to sudden changes in environmental iron, such as those that occur during mammalian infection, *A. fumigatus* has evolved a complex iron regulatory network. Iron regulatory proteins receive input about both intra- and extra-cellular iron and communicate commands to iron uptake, storage, and usage systems through feedback loops. In this section I will discuss in detail each node in the network and give a list of model assumptions which were made either for simplicity or due to insufficient information.

3.1 Model Components

There are five main components to the model: siderophore biosynthesis (SB), iron acquisition, iron storage and distribution, iron consumption, and iron regulatory proteins (See Figure 4.1).

Siderophore Biosynthesis:
A. fumigatus produces four siderophores, low molecular mass ferric iron-specific chelators [6]. The two extracellular siderophores, fusarinine (FsC) and its derivative triacetylfusarinine C (TAFC) are excreted from the cell after synthesis to sequester iron from the external environment. The two intracellular siderophores, ferricrocin (FC) and its derivative hydroxyferricrocin (HFC) are used for hyphal iron storage and conidial iron storage, respectively. Additionally, FC has been shown to participate in transcellular iron distribution [8]. For simplicity, the model considers only the siderophores TAFC and FC, which have been shown to be the two most abundant and active siderophores [17]. The first step in the biosynthesis of all four siderophores is the hydroxylation of ornithine catalyzed by SidA, an ornithine monoxygenase. The biosynthesis of ornithine is upregulated by HapX during iron limitation [4]. After this step the pathways for siderophore biosynthesis split into two pathways, one that catalyzes the assembly of extracellular siderophores and another pathway that catalyzes the assembly of intracellular siderophores. Siderophore biosynthesis is essential for full virulence of *A. fumigatus* during mammalian infection. In fact, a SidA mutant strain was shown to be avirulent in a mouse model of invasive aspergillosis [11] [10]. Other enzymes in the SB pathway have been characterized [2]; however, as SidA initiates the entire siderophore biosynthesis process, only SidA is modeled and not any of the enzymes involved in SB once the pathway splits.

Iron acquisition:
Mechanisms of iron excretion have not been found in fungi [13]. Therefore iron acquisition is believed to be the main iron homeostasis control mechanism in *A. fumigatus*. *A. fumigatus* has three known mechanisms of iron uptake: low affinity ferrous iron uptake and two high affinity ferric iron

uptake systems. Low affinity iron uptake has not yet been characterized at the molecular level for any fungal species other than *Saccharomyces cerevisiae*, so this uptake mechanism is not included in the model [3]. The iron acquisition model component includes only the two high affinity iron uptake systems, namely siderophore-mediated iron uptake and reductive iron assimilation (RIA). The first step in RIA is the reduction of ferric iron to the more soluble ferrous iron by ferric reductase FreB [16]. The ferrous iron is then re-oxidized and imported by a protein complex consisting of the ferroxidase FetC and the iron permease FtrA [10]. For modeling purposes, these three proteins are accounted for in a single variable called RIA. In a mouse model of *Aspergilus* infection RIA was not shown to play a crucial role in virulence [10]. Therefore RIA plays a limited role in the model. Siderophore-mediated iron uptake is represented by nodes TAFC, MirB, and EstB. TAFC, the main extracellular siderophore, is released into the environment to steal ferric iron from host transferrin [18]. Upon chelation of Fe(III) by TAFC outside the cell, the ferri-TAFC complex is taken back up. A protein family called siderophore-iron transporters (SIT) recognizes and retrieves specific ferri-siderophores. The SIT MirB has been shown to be specific to TAFC. It is interesting to note that SIT are one of the few protein families that are unique to fungi, hence the family may include potential drug targets. After import into the cell the ferri-TAFC complex is degraded by an esterase, EstB, and iron is subsequently released into the cell for transcellular distribution and storage [7].

Iron Storage:
Unlike bacteria, plants and animals, most fungi lack ferritin-mediated iron storage [13]. Instead, *A. fumigatus* relies on siderophore-mediated iron storage and distribution, via the intracellular siderophore FC and a siderophore-independent iron storage unit, the iron vacuole [8] [19]. The importance of FC for intracellular iron transport is evidenced by the fact that FC deficiency results in iron-starved conidia, asexual fungal spores which depend on nutrient transport [8] [9]. Import of iron into the vacuole is in part mediated by the protein CccA which is localized in the vacuolar membrane. Expression of CccA is upregulated by iron [19]. In the model, CccA is represented implicitly in the node VAC which tracks the amount of iron stored in the vacuole. This node may include other iron importers, as it was shown that CccA does not exclusively control vacuolar iron storage [19]. Again, since fungi lack mechanisms for iron excretion, iron storage plays a crucial role in iron detoxification.

Iron Consumption:
Currently, iron consumption is represented as a "black box." The model does not account for any specific modes of iron consumption, but rather joins them all together. The reason for this generality is: (1) I am concerned only with whether intracellular iron is or is not being depleted at a given time, not with how it is depleted, and (2) for the purposes of model simplicity I do not consider possible effects on iron regulatory proteins by the use or lack of use of iron by iron-dependent systems. This box includes iron-dependent systems such as heme biosynthesis, TCA cycle, respiration, ribosome biogenesis, etc. that are down regulated by transcription factor HapX under low iron conditions [3].

Regulatory Proteins:
Iron regulation in *A. fumigatus* is tightly controlled by two central transcription factors: the bZip-factor HapX and the GATA-factor SreA. HapX is repressed by iron whereas SreA is upregulated by iron. Iron regulates both SreA and HapX posttranslationally by blocking HapX function and activating SreA function [2]. During iron starvation HapX represses iron-consuming pathways, such as heme biosynthesis, TCA cycle, and respiration and upregulates iron acquisition pathways such as siderophore biosynthesis (SB), reductive iron assimilation (RIA), and siderophore uptake.

Iron-dependent pathways are repressed by physical interaction of HapX with CCAAT-binding core complex [3]. HapX activates siderophore biosynthesis partly by upregulating the production of ornithine, the SB precursor [4]. During iron sufficiency SreA represses iron uptake systems, such as RIA, SB, and ferri-siderophore import, to avoid toxic effects of excessive iron [1]. Since HapX is active during iron starvation, growth defects due to HapX inactivation are restricted to iron deplete conditions. On the other hand, since SreA is active during iron sufficiency, growth defects due to SreA inactivation are restricted to iron replete conditions. Furthermore, SreA and HapX influence each other's expression via a double negative feedback loop. SreA represses HapX during iron sufficiency while HapX represses SreA during iron starvation. Simultaneous inactivation of both SreA and HapX is synthetically lethal [4]. There is evidence that *A. fumigatus* likely senses iron through other regulatory proteins [2]. For example, the sterol regulatory element binding protein (SREBP) SrbA which is involved in hypoxic adaptation has been found to activate iron uptake in part by transcriptional activation of HapX [14]. However for the purposes of model simplicity, only the regulatory proteins HapX and SreA are considered.

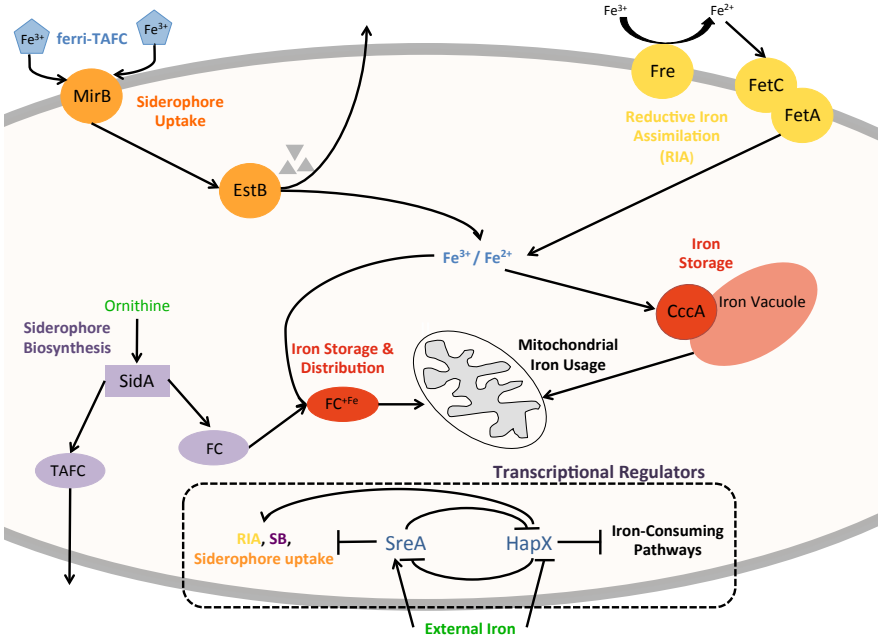

Figure 3.1: Iron regulatory network in *A. fumigatus*.

3.2 Summary of Model Assumptions

1. Iron regulatory proteins, HapX and SreA, "sense" iron both externally and internally. This is represented in the model by the fact that the update rules of variables for HapX and SreA depend on the Environmental Iron node and CccA/Iron Vacuole node (VAC).

2. The second high-affinity iron uptake system, reductive iron assimilation (RIA), only makes a significant contribution to iron uptake under high iron conditions, i.e. RIA has no effect on model dynamics under low iron conditions. This is justified by the fact that siderophore-mediated iron uptake is much stronger than RIA as is evidenced by the fact that an *A.*

fumigatus mutant lacking siderophore biosynthesis, but not a mutant lacking RIA, is avirulent in a mouse model [10].

3. The model does not account for any direct interaction with host iron such as iron bound to transferrin or other host proteins. Rather, it is assumed that once TAFC is synthesized a certain amount, depending on the external concentration of iron, of ferri-TAFC automatically "arrives" for retrieval by the cell. Thus, if external iron is low then few TAFC-Fe complexes will arrive. If external iron is high, then many TAFC-Fe complexes will arrive.

4. It is not known by what method siderophores are excreted by the cell [3]. Hence it is assumed that if TAFC is synthesized, then it is outside the cell. This and the previous assumption essentially manifests in the model in that there is no time delay between synthesis and import of ferri-TAFC.

5. After being released into the cell by hydrolysis of siderophore backbones via EstB, iron must first "enter" one of the two storage units before becoming available for consumption. Therefore there is no arrow directly from EstB to ICP. The paths iron can take are either EstB $\rightarrow$ FC $\rightarrow$ ICP or EstB $\rightarrow$ VAC $\rightarrow$ ICP.

6. MirB is the only siderophore iron transport (SIT) capable of importing TAFC into the cell. Thus in the model, if MirB is inactive then no siderophore-iron complex can be brought into the cell. Even though MirB is the only SIT shown to be TAFC specific, that may not be a true portrait of reality, as ten putative *A. fumigatus* SITs have been identified with predicted overlapping specificity [21] [2].

7. Only two of the four native siderophores are modeled. No xenosiderophores are modeled.

8. Release of iron captured by siderophore-mediated uptake into the cell is dependent upon hydrolysis of TAFC-Fe complex by EstB. This is not entirely biologically accurate as it has been shown that EstB-mediated TAFC hydrolysis optimizes but is not essential for TAFC-mediated iron uptake in *A. fumigatus* [7].

9. Once TAFC is synthesized and excreted from the cell, it remains "available" outside the cell until it is taken up by the SIT, MirB. This explains why MirB is an input to the function for TAFC.

Chapter 4

Mathematical Model

4.1 Nodes and State Discretizations

The model presented here is a literature-based discrete dynamical system. It is literature-based in the sense that a collection of known (published in the literature) regulatory interactions have been integrated into a dynamic framework. This is one common approach to characterizing complex molecular networks. Iron regulation in *A. fumigatus* has been well studied. In fact, *A. fumigatus* is considered a model filamentous fungus and claims a robust international research community. Recently, a first step in the direction of modeling iron homeostasis in *A. fumigatus* was made by one of the leading research groups in this field [15]. Figure 4.1 is the wiring diagram describing which nodes in the network interact with each other and whether they interact in an inhibitory or activating manner. $A \to B$ means node A activates node B. On the other hand $A \dashv B$ means node A inhibits node B. Note that nodes VAC and FC have self-activating arrows. This is to account for the fact that iron storage levels, in the vacuole for instance, should not jump from high storage to no storage in a single time step. Iron levels in the vacuole must go from high vacuolar iron (state 2) to low vacuolar iron (state 1) to no vacuolar iron (state 0) but not from state 2 to state 0, for example, in one time step. The pale pink circle represents the fungal cell. Proteins such as MirB and those involved in RIA are localized on the cell membrane. Other than the distinction among "inside the cell", "outside the cell", and "on the cell membrane," the location of nodes in the network is arbitrary and meaningless.

Recall that the wiring diagram is merely a static snapshot of the network. To obtain a dynamic model logical rules governing the update of each node must be specified, for instance in a transition table. But first, a discretization of variable states must be determined. Table 4.1 gives the list of model variables, their function in the iron regulatory network, number of states, and biological descriptions of each state. Note that most variables are Boolean. When choosing the number of variable states the discretization should be fine enough to accurately capture biological phenomena. On the other hand, there should be as few discrete states as possible for the purposes of model simplicity. Also note that the elements $0, 1, 2$ can have different biological meanings for different variables.

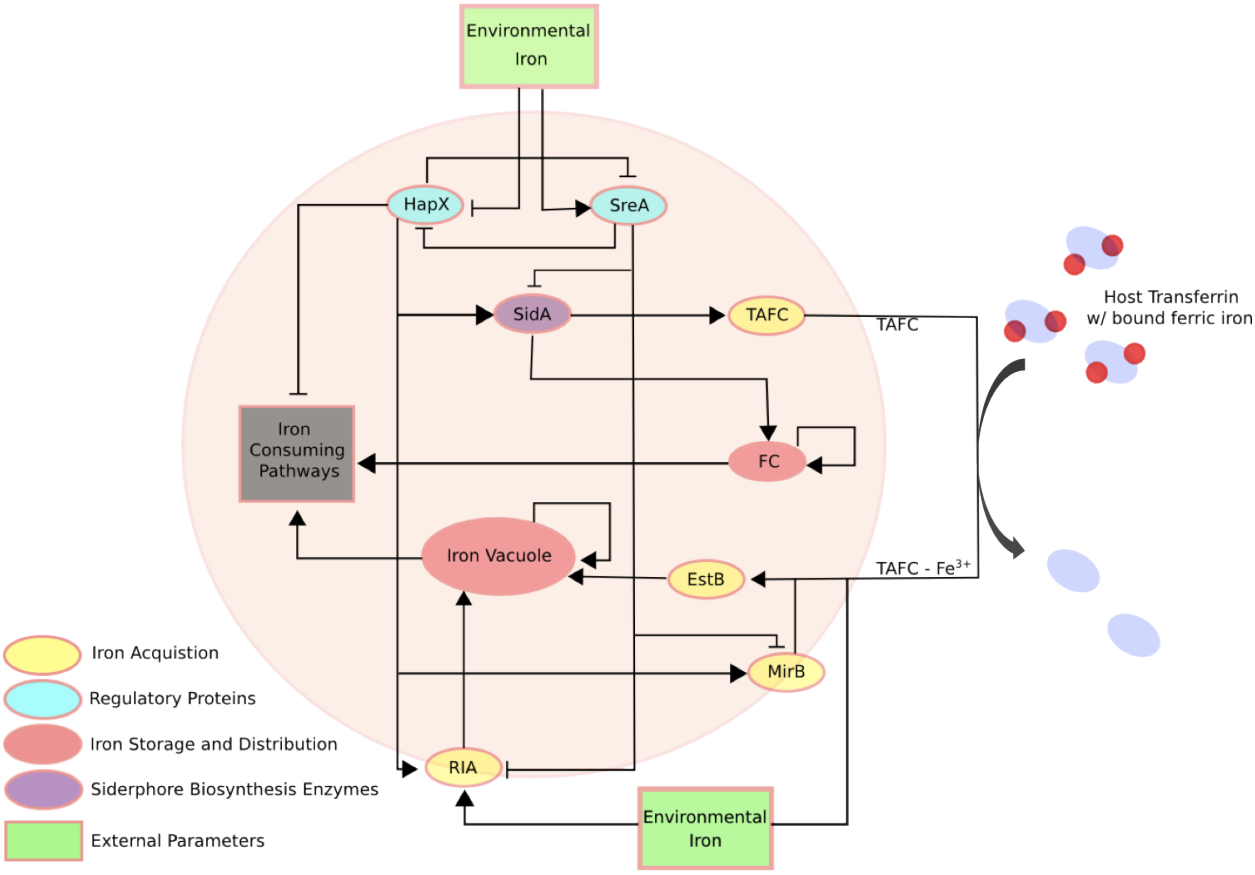

Figure 4.1: Wiring diagram: Each oval or rectangle is a variable in the model. The arrows describe how variables interact with each other.

Variables	Function	Biological State Descriptions		
		0	1	2
Iron	external parameter	low iron	high iron	x
HapX	regulatory protein	inactive	active	x
SreA	regulatory protein	inactive	active	x
SidA	catalyzes first step in SB	no hydroxylation of ornithine	hydroxylation of ornithine	x
RIA	high affinity iron uptake	insignificant iron contribution	significant iron contribution	x
TAFC	extracellular siderophore	unsynthesized	synthesized	x
MirB	TAFC SIT	ferri-TAFC import disabled	ferri-TAFC import enabled	x
EstB	TAFC esterase	no hydrolysis	hydrolysis releasing low iron	hydrolysis releasing high iron
FC	intracellular siderophore	unsynthesized	synthesized	synthesized and carrying iron
VAC	vacuolar iron storage	no vacuolar iron	low vacuolar iron	high vacuolar iron
ICP	iron consuming pathways	no iron consumption	low iron consumption	high iron consumption

Table 4.1: State descriptions of network nodes.

4.2 Iron Levels

To incorporate the ability of iron regulatory proteins HapX and SreA to sense iron levels from both inside and outside the cell, it was necessary to determine what configurations of external iron concentration and internal iron stored in the vacuole lead to a state of "iron starvation" or "iron sufficiency". "Iron starvation" and "iron sufficiency" are defined in the following way:

Ext. Iron	VAC	Iron Status
0	0	starvation
0	1	starvation
0	2	starvation
1	0	starvation
1	1	starvation
1	2	sufficiency

Table 4.2: Iron starvation and sufficiency levels.

Note that there is only one state of iron sufficiency among the six configurations. This decision was made based upon the context in which *A. fumigatus* is usually studied. During mammalian infection, the fungus is in a state of iron starvation as the host immune response seeks to deprive the fungus of iron. Therefore there is a finer discretization of levels of iron starvation whereas iron sufficiency and iron overload are grouped into the same category. These states are arbitrarily chosen, however based upon results reported by Power *et al.* (Figure 2(B)) [5], the starvation states may fall roughly between 0 and 10 μM iron concentrations while the iron sufficiency state corresponds to an iron concentration between 10 and 100 μM.

In the model, when the fungus is in a state of iron starvation as defined in Table 4.2, HapX is activated unless SreA is active. If SreA is active, it has an inhibitory effect on HapX and hence HapX will be inactive regardless of iron conditions. Otherwise, if the fungus is in a state of iron sufficiency, then SreA is activated unless HapX is active. In this case, HapX has an inhibitory effect on SreA and hence SreA will be inactive regardless of iron conditions. Recall that HapX and SreA are connected by a double negative feedback loop. Defined in this way, it can never occur at any time step (unless we start with an initialization already in this configuration) in the model that both HapX and SreA are active. Note that it has been reported that in *A. nidulans*, inactivation of both HapX and SreA is synthetically lethal [20].

4.3 Transition Tables

Each of the network variables listed in Table 4.1 is assigned a set of "rules" or functions that describe how the node will be updated at the next time step based upon the states of that node's inputs at the current time step. It is convenient to represent this information in a transition table. In the Mathematical Background section transition tables were explained for a synthetic system. The following example will show how to extract logical rules or build transition tables from biological information in the literature. For example suppose the following summary is extracted from the literature:

> The amount of iron scavenged by siderophore-mediated iron uptake mechanisms and made available for use by the cell via hydrolysis of siderophore backbones is dependent upon the amount of iron outside the cell, the synthesis and excretion of extracellular

> siderophores, and the activity of siderophore iron transporters which sit on the cell membrane and are responsible for bringing siderophore-iron complexes into the cell.

From this statement, the following simple logical rules for node EstB can be inferred:

low iron + active MirB + TAFC ⇒ hydrolysis; low iron released
high iron + active MirB + TAFC ⇒ hydrolysis; high iron released
else ⇒ no hydrolysis; no iron released

Of course there is no one correct way to interpret and represent the literature. This is just one possible implementation. The logical rules can then be encoded into a transition table which specifies for each configuration of the states of inputs to EstB an output state of EstB at the next time step. The inputs to EstB are simply the nodes which have edges incident to node EstB in the wiring diagram in Figure 4.1. These nodes are Iron, MirB, and TAFC as listed in the logical rules. Note from Table 4.1 that nodes Iron, MirB, and TAFC are all boolean meaning that at any given time they can be in one of two states. Therefore, there are $2^3 = 8$ possible configurations of these three nodes. Note that EstB, however, has 3 states. Therefore the fact that the input nodes are boolean does not mean that EstB also needs to be boolean. The transition table for EstB is shown in Tables 4.3 and 4.4. In Table 4.3 the states of each node are described verbally. In Table 4.4, these words have been translated into numbers. For a full list of transition tables see the Appendix A.1.

Iron(t)	MirB(t)	TAFC(t)	EstB(t+1)
low	inactive	not synthesized	no hydrolysis
low	inactive	synthesized	no hydrolysis
low	active	not synthesized	no hydrolysis
low	active	synthesized	hydrolysis; low iron
high	inactive	not synthesized	no hydrolysis
high	inactive	synthesized	no hydrolysis
high	active	not synthesized	no hydrolysis
high	active	synthesized	hydrolysis; high iron

Table 4.3: Example transition table: EstB

⇓

Iron(t)	MirB(t)	TAFC(t)	EstB(t+1)
0	0	0	0
0	0	1	0
0	1	0	0
0	1	1	1
1	0	0	0
1	0	1	0
1	1	0	0
1	1	1	2

Table 4.4: Transition table for EstB converted to numbers.

Once a transition table is constructed for each variable in the network, all possible interactions are specified. If the model is small enough, dynamic behavior can now be simulated. By following all possible initial configurations, one obtains a complete description of the dynamics of the model such as steady states, oscillatory behavior, or the size of the basins of attraction. In general the model is too complex to be analyzed in this exhaustive way. At this point the discrete model, in the form of transition tables, is translated into a mathematical object, in the form of polynomial dynamical systems, so that rigorous mathematical theory can be applied.

4.4 Mathematical Framework - PDS

For analysis purposes discrete models are represented as mathematical objects within the framework of polynomial dynamical systems (PDS), a system of polynomial equations over a finite field. Once a discrete model has been converted to PDS form one can apply theory from abstract algebra and tools from computational algebra to analyze the dynamic features of the system such as steady states and limit cycles.

Recall the definition of a polynomial dynamical system, Definition 2.8. The variables x_i are the network nodes listed in Table 4.1. The coordinate functions f_i are interpolated from the transitions table for node x_i and encode all the information stored in the tables. The elements in the field k must contain as a subset the set of states of the node with the greatest number states. In the case of this model, the greatest number of states for any node is 3 as can be seen in table 4.1. Therefore our finite field must contain elements $0, 1, 2$. The smallest field satisfying this criterion is $\mathbb{F}_3 = \{0, 1, 2\}$. The interpolating function introduced with Definition 2.8 in the Mathematical Background section is used to construct a function for each node x_i, for $i = 1, ..., 11$.

In the above example, the polynomial interpolation of the transition table for node EstB is:

$$f_{EstB} = Iron * MirB^2 + Iron * MirB^2 * TAFC + Iron * MirB * TAFC^2 +$$

$$MirB^2 * TAFC^2 + Iron * MirB * TAFC + MirB^2 * TAFC + MirB * TAFC^2 + MirB * TAFC$$

The model presented here can be described either by 10 transition tables subject to the external parameter, Iron, or within the framework of polynomial dynamical systems:

$$F = (f_1, ..., f_{11}) : \mathbb{F}_3^{11} \to \mathbb{F}_3^{11}$$

where the $f_i \in \mathbb{F}_3[x_1, ..., x_{11}]$ are the polynomials interpolated from transition tables.
See Appendix A.2 for a complete list of polynomials.

Chapter 5

Analysis and Simulation

5.1 Steady State Analysis - Iron Deplete

To analyze the model, equilibrium solutions were calculated. Depending on whether iron in the external environment is high (Iron=1) or low (Iron=0) the fungus' iron regulatory system will come to rest in one of two equilibrium solutions. If environmental iron is low or depleted, the model will settle at a single steady state characterized by an active siderophore system, no internal iron storage, and low mitochondrial iron consumption. This low iron steady state behavior has been reported in several places [1] [5] [4] [19]. The low iron steady state of each node in the network is listed in Table 5.1 and presented as a bar graph in Figure 5.1. On the other hand, if environmental iron is high the model predicts oscillatory steady state behavior. This iron replete steady state will be discussed in detail in Section 5.3.

Variables	Function	Iron Deplete Steady State
Iron	external parameter	low
HapX	regulatory protein	active
SreA	regulatory protein	inactive
SidA	catalyzes first step in SB	hydroxylation of ornithine
RIA	high affinity iron uptake	insignificant iron contribution
TAFC	extracellular siderophore	synthesized
MirB	TAFC SIT	ferri-TAFC import enabled
EstB	TAFC esterase	hydrolysis releasing low iron
FC	intracellular siderophore	synthesized; no iron
VAC	vacuolar iron storage	low vacuolar iron
ICP	iron consuming pathways	low iron consumption

Table 5.1: Iron deplete steady state.

In the iron deplete steady state regulatory protein HapX is active while SreA is inactive. HapX activates siderophore-mediated iron uptake - SidA and MirB. RIA can also be thought of as being activated, however under low iron conditions this iron uptake mechanism does not make a significant contribution to iron acquisition. SidA catalyzes the first step in the biosynthesis of extracellular and intracellular siderophores, TAFC and FC respectively. Node EstB is in state 1 (low iron released), rather than state 2 (high iron released), because under low iron conditions TAFC can only sequester a small amount of iron. Due to this, FC is only active but not bound to any iron (state 1) and VAC is storing only small amount of iron (state 1). Since FC has no iron content in this steady state it cannot facilitate the intracellular transport or distribution of iron to conidia, asexual fungal spores. In real fungal cells, this situation results in iron starved conidia and delays germination during iron starvation [2]. The iron consuming pathways variable, ICP, is in a state of low iron consumption (state 1) due in part to low intracellular iron stores and the fact that HapX inhibits ICP in iron limiting environments.

5.2 Knockout Analysis

Siderophore biosynthesis has been shown to be essential for *A. fumigatus* virulence in a murine model of invasive aspergillosis [10] [11]. In an experiment conducted by Schrettl *et al.* wild type and mutant strains of *A. fumigatus* were point inoculated on AMM plates containing varying

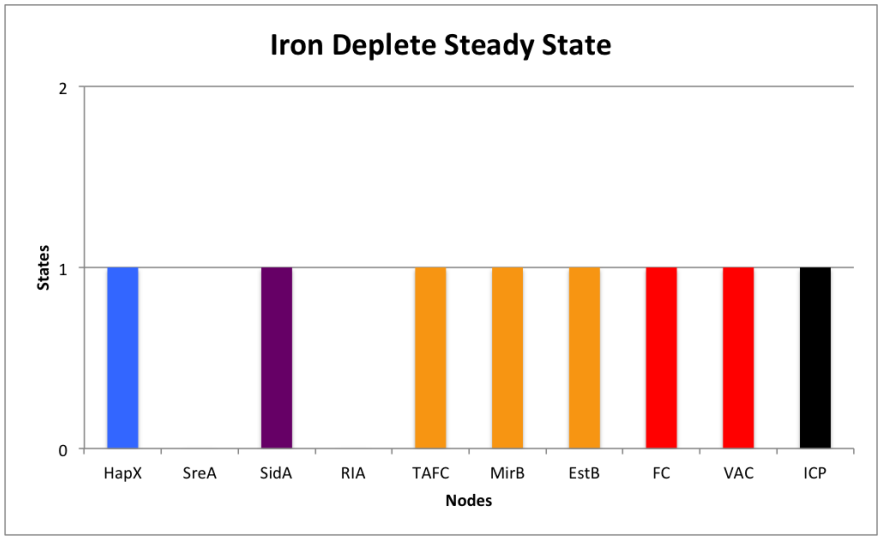

Figure 5.1: Iron deplete steady state.

concentrations of iron and incubated at 37°C for 48 hours [10]. The results showed that in iron depleted conditions the SidA mutant showed hardly any radial growth. Under iron replete conditions $\Delta sidA$ showed some radial growth but to a much lesser degree than the wildtype under the same conditions. A double mutant $\Delta sidA\Delta ftrA$, in which both high affinity iron uptake systems are knocked out, was unable to grow at all unless supplemented with siderophores and high iron. The behavior of both mutants under high and low iron environmental iron conditions is reflected in the model by associating radial growth with ICP, VAC, and FC. To simulate a SidA knockout, the model was analyzed under the assumption that variable SidA = 0. It was also assumed that no siderophores had been synthesized prior to knockout, i.e. FC and TAFC were initialized to 0. The double knockout $\Delta sidA\Delta ftrA$ is equivalent to $\Delta sidA\Delta$RIA in the model. Figure 5.2 shows steady state results from model knockout simulations. The values of VAC, FC, and ICP in the model correlate with the amount of growth one would expect to see experimentally. Note that under low iron conditions neither $\Delta sidA$ nor $\Delta sidA\Delta$RIA show significant growth since FC = VAC = ICP = 0. Under iron replete conditions $\Delta sidA$ grows at a rate similar to the wild type under iron deplete conditions. $\Delta sidA\Delta$RIA still shows no growth even in iron replete conditions. Note that in a high iron environment, vacuolar iron storage (VAC) and iron consumption (ICP) are only somewhat higher than in the $\Delta sidA$ mutant. However a significant difference is that FC is carrying more iron as compared to the $\Delta sidA$ mutant and wildtype fungus under iron deplete conditions in which FC is either not present or not bound to iron, respectively. Recall that FC is important to intracellular iron transport, especially to condia. FC deficiency was shown to cause iron starvation in conidia and reduce conidial germination efficiency [2]. Therefore model behavior agrees with the fact that *A. fumigatus* shows more growth under iron replete conditions.

5.3 Steady State Analysis - Iron Replete

5.3.1 Analysis of Deterministic Model

In an iron replete environment (Iron=1) the model predicts oscillatory steady state behavior. Figures 5.3a and 5.3b show a sample trajectory in which the model is initialized in the low iron steady

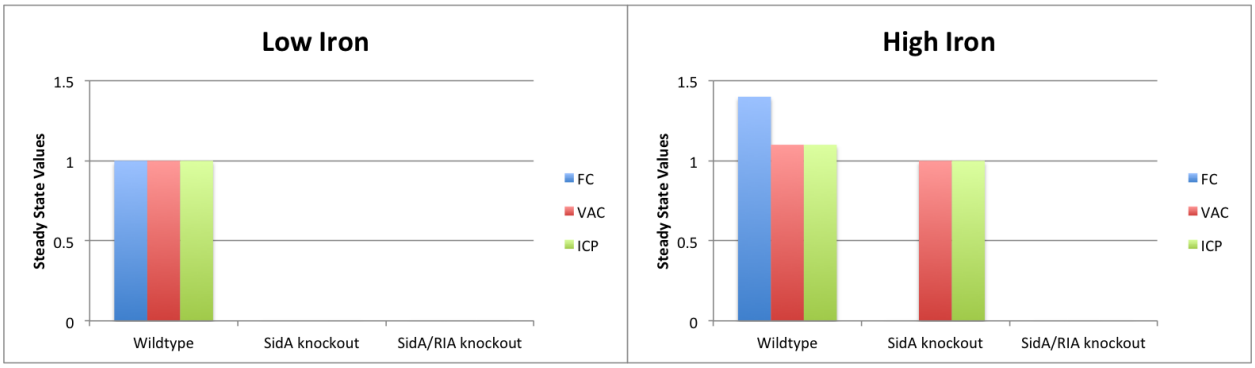

Figure 5.2: Steady state results for wildtype, $\Delta sidA$ and $\Delta sidA\Delta$RIA for Iron $= 0, 1$.The wild-type behavior under high iron conditions is the average over all states in the high iron limit cycle.

state (Table 5.1) and subsequently iron is fixed at high for the remainder of the simulation. Initially siderophore iron uptake is activated (HapX=1, SidA=1) and the fungus begins acquiring and storing iron (VAC=2).The model arrives at the limit cycle at time step 3. Around time step 6 the fungus has acquired enough iron from the environment via iron uptake systems and shuts off those systems (SreA=1, SidA=0). At this point the fungus has sufficient intracellular iron stores and begins consuming those iron stores at a higher rate (ICP=2). As intracellular iron stores are depleted (VAC=1,0) iron consumption decreases (ICP=1,0) and high affinity iron uptake systems are re-induced (SreA=0, HapX=1, SidA=1). As long as environmental iron content remains high, the model lives in this limit cycle characterized by periods of iron uptake followed by iron storage, consumption of available intracellular iron, and finally re-induction of high-affinity iron uptake.

Note how time delay is captured by the discrete framework due to a series of intermediaries involved in the feedback loop between the transcription factors, HapX and SreA, and intracellular iron stores (VAC). At time step 4 intracellular iron stores are at full capacity, and the gene coding for HapX becomes inactive. Yet there is still protein HapX around until time step 5. At time step 4 there is plenty of intracellular iron, yet SreA does not appear until time step 6. This time delay in the model is capturing the biological time delays inherent in genetic control such as the delay between the start of transcription and the end of translation. At time step 4, the gene coding for SreA should be activated, yet protein HapX is still present which inhibits the transcription of SreA. We can infer that transcription of SreA starts at time step 5, yet protein SreA does not appear until time step 6. Delays essentially occur in the model because a variable must wait for its input variables to be updated before it can update, and only one update occurs per time step. One can observe the delays propagate throughout the time course. For example, regulatory protein HapX appears again at time step 10, yet SidA does not become active until the following time step.

5.3.2 Stochastic Simulations

Until this point, the model analyzed is a deterministic discrete dynamical system with synchronous update schedule. Recall that synchronous updating means that all nodes or proteins are updated at the same time. Steady states are preserved regardless of update schedule. Limit cycles, however, may be different as the model becomes increasingly non-deterministic. In order to verify that the steady state oscillations observed in this analysis were not an artifact of the deterministic framework, the model was also analyzed with an update schedule obeying a uniform random distribution.

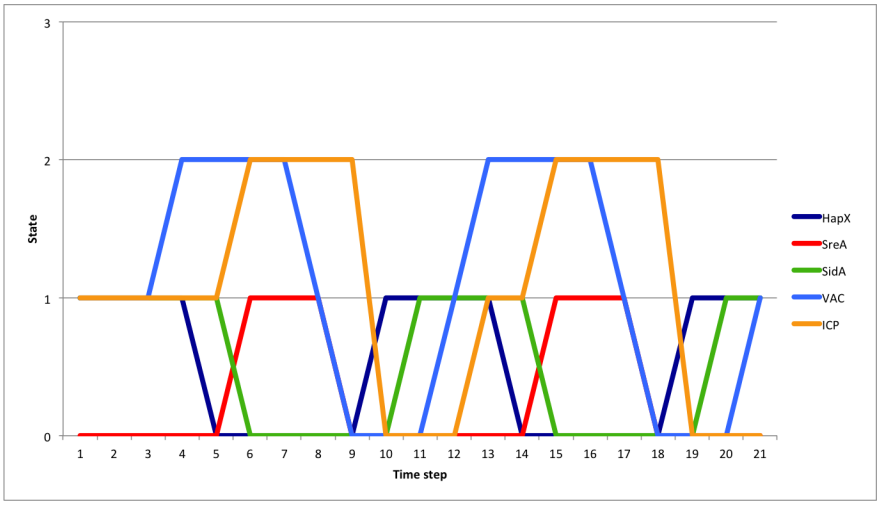

(a) Sample trajectory of transcription factors HapX and SreA, storage unit VAC, iron consumption node ICP, and siderophore mediated iron uptake SidA. Environmental iron is fixed at high.

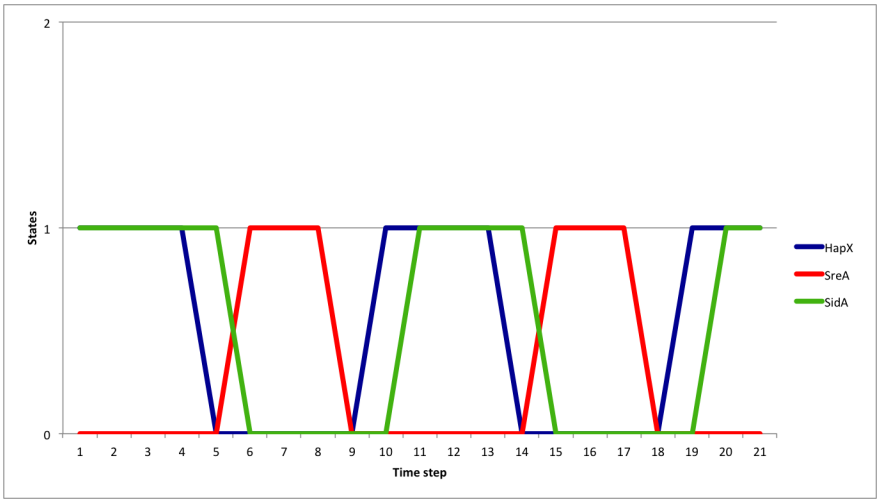

(b) A closer look at HapX, SreA, and SidA in the same trajectory as (A).

Figure 5.3: Deterministic trajectories from the low iron steady state into the high iron limit cycle.

To implement this update schedule the model was embedded into the stochastic discrete dynamical systems (SDDS) framework discussed in Section 2, (Definition 2.12). Within this framework an update schedule following a uniform random distribution translates to a propensity matrix in which all entries are 0.5. This means that at each time step any given node is equally likely to be either updated according to the rules in its transition table or remain in its current state. I start with this uniform random distribution because little quantitative information is known about speed of reactions in the iron regulatory network. Figures 5.4a and 5.4b show that oscillations are preserved in this framework, and hence the oscillatory steady state behavior is robust to update schedule.

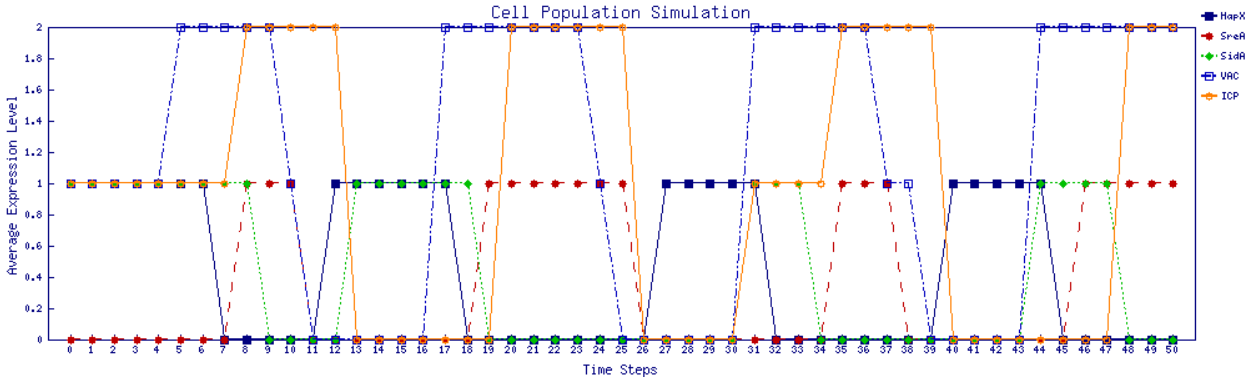

(a) Sample stochastic trajectory of transcription factors HapX and SreA, siderophore mediated iron uptake SidA, storage unit VAC, and iron consumption node ICP. The model is initialized from the low iron steady state with environmental iron fixed at high.

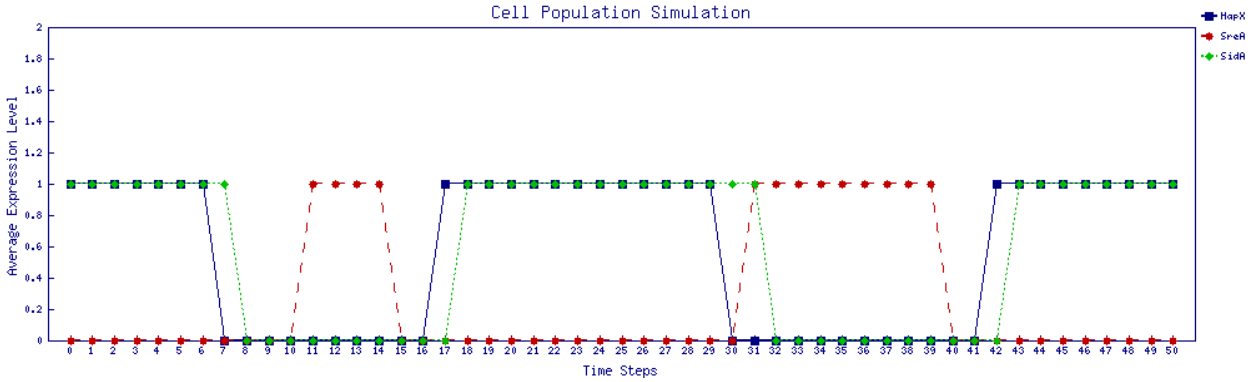

(b) Sample stochastic trajectory of transcription factors HapX and SreA and siderophore mediated iron uptake SidA. The model is initialized from the low iron steady state with environmental iron fixed at high.

Figure 5.4: Stochastic trajectories on a single cell population with random updating.

5.3.3 Multi-cell Population Simulations

In a non-deterministic framework single cell simulations (trajectory of a single simulation) may behave differently from multi-cell populations (average trajectory over many simulations). This occurs because a non-deterministic update schedule allows for variations among individual simulations. This is biologically analogous to individual cells in a population getting out of sync with each other. Figures 5.5a and 5.5b show that iron replete steady state oscillations are sustained in a single cell, but oscillations are damped in a multi-cell population. For both the single cell and multi-cell simulations, all cells are initially in sync in the low iron steady state shown in Table 5.1.

There is some evidence in the literature for oscillatory behavior in a high iron environment. Schrettl *et. al.* investigated the influence of iron on the expression of several genes in the network discussed here: *sidA*, *sreA*, *cccA* (corresponding to VAC), *cat1* (corresponding to ICP), and genes involved in RIA [1]. In an *in vitro* shift experiment from iron deplete to iron replete conditions, they observed in wild-type *A. fumigatus* an initial increase in transcript levels relating to iron uptake systems, a dramatic decrease in these transcript levels in the middle of the time course, and finally a slight increase in transcript levels toward the end of the time course. This experiment gives some indication that model-predicted oscillatory steady state behavior is an accurate representation of the biological system. Independent model validation of this prediction is discussed in the following sections.

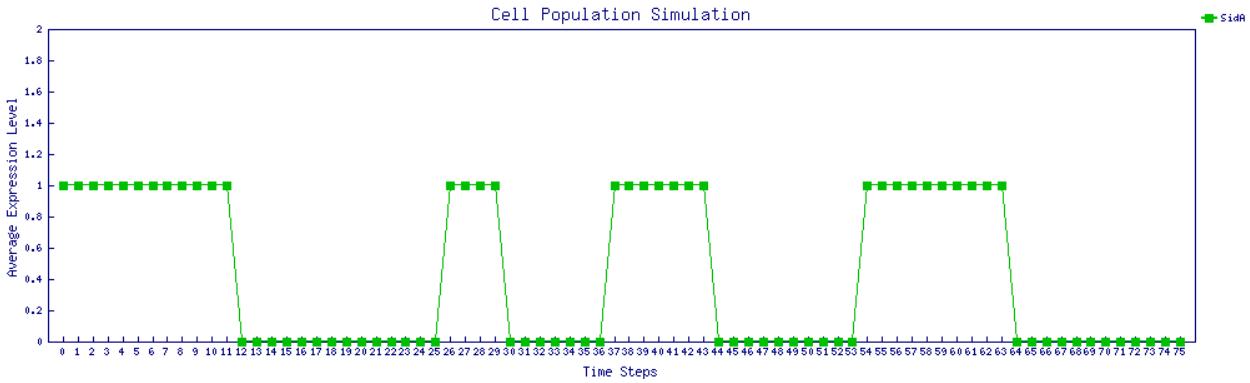

(a) Sample stochastic trajectory under random updating of siderophore mediated iron uptake node, SidA, in a single cell population. Oscillations are sustained. The model is initialized from the low iron steady state with environmental iron fixed at high.

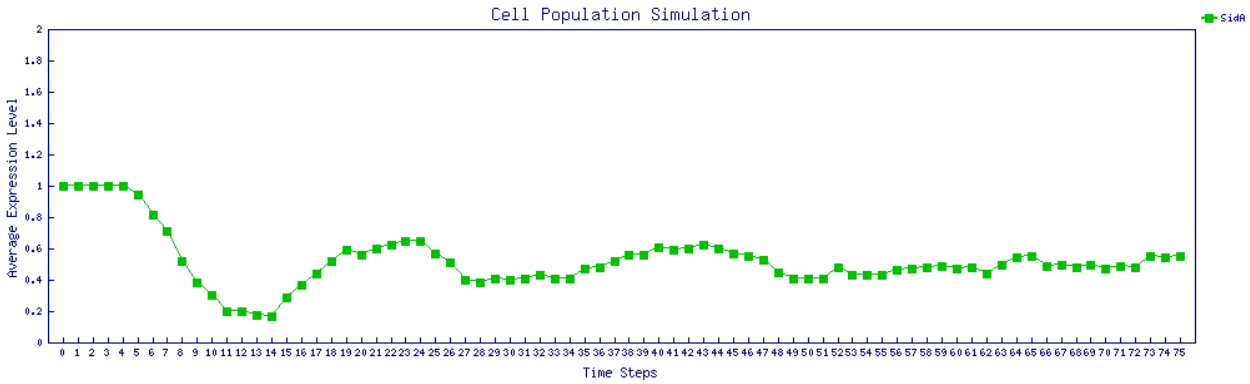

(b) Sample stochastic trajectory under random updating of siderophore mediated iron uptake node, SidA, in a population of 100 cells. Oscillations dampen over time in the 100 cell population. The model is initialized from the low iron steady state with environmental iron fixed at high.

Figure 5.5: Stochastic trajectories with a uniform random distribution of update schedules in a switch from low to high iron environment.

Recently, damped oscillations in expression of genes involved in iron homeostasis in a single *E. coli* cell in a switch from an iron replete to an iron depleted environment were discovered using single-cell experiments and modeled using differential equations [36]. To investigate whether *A. fumigatus* also exhibits this behavior, I ran both single cell and 100-cell stochastic simulations subject to a uniform randomly distributed update schedule in which the fungal cells are initialized in a state of high external and internal iron and are subsequently switched to an iron depleted environment. In this switch, the model predicts initial very slight oscillations before arriving at the low iron steady state. Plots of this prediction are included in Appendix A.3 (Figures A.1a and A.1b). Damped oscillations in a switch from an iron replete to an iron depleted environment are not experimentally investigated in this work.

Chapter 6

Experimental Methods

Strain and growth conditions: The *Aspergillus fumigatus* strain used was wild-type AF293. *A. fumigatus* was cultured on glucose minimal media plus agar plates at 37°C for 7 to 10 days until fully conidiated. Spores were harvested by flooding the culture plates with endotoxin-free phosphate-buffered saline solution containing 0.05% Tween-20 and swabbing with a sterile inoculation loop to obtain spore suspension. The spores were vortexed and concentrations of spores were determined by counting in a hemacytometer.

Incubation: *A. fumigatus* was grown in a liquid shaker under iron depleted conditions. 25 million *A. fumigatus* condia were added to standard glucose minimal media (1L formula - 50 mL 20X salt solution, 1 mL trace elements, 10 g D-glucose (Dextrose), 15 g agar) plus 0.05% Tween-20 but without iron in the trace elements to a final volume of a 25 mL for a final concentration of 1 million spores per mL. Flasks were incubated at 37°C and 200 rpm for 84 hours. Glass flasks were rinsed prior to inoculation with a 0.1 M HCL solution followed by a rinse with double distilled water to remove residual traces of iron. After 84 hours, *A. fumigatus* was shifted from iron depleted to iron replete conditions by adding $FeSO_4$ to a final concentration of 10μM $FeSO_4$. *A. fumigatus* was then incubated for another 9.5 hours.

Harvesting: Mycelia were harvested from triplicate samples at 0, 10, 60, 120, 240, 300, 330, 360, 390, 420, 450, 480, 510, 540, and 570 minutes after the addition of iron. Mycelia were filtered through gauze and immediately flash frozen in liquid nitrogen and stored at -80°C. Frozen mycelia were subsequently ground to a fine powder using a mortar and pestle in the presence of liquid nitrogen.

RNA extraction, cDNA synthesis:
Total RNA was isolated using a Qiagen RNeasy plant mini-kit. "Protocol: Purification of Total RNA from Plant Cells and Tissues and Filamentous Fungi" was used along with optional on-column DNase digestion step. Extracted RNA was stored at -80°C. RNA integrity was assessed by gel electrophoresis. The gel consisted of 1 gram agarose powder, 100μL 1×TAE, and 3μL ethidium bromide. 3μL of RNA sample was added to 1μL 6× loading dye and 6μL formamide and loaded onto the gel. See Appendix A.4 (Figure A.4) for an image of the gel. Concentrations of RNA in each sample were determined by spectrophotometry on a NANODROP 1000 Spectrophotometer. Next, cDNA was synthesized following manufacturer's instructions (Tetro cDNA Synthesis Kit, Bioline). All incubations were carried out in a thermacycler. Following synthesis, cDNA was stored at -20°C.

Real time qRT-PCR:
Real time reverse transcriptase polymerase chain reaction (qRT-PCR) was performed using the cDNA as a template. The constitutively expressed gene β-tubulin of *A. fumigatus* was used as the house-keeping gene. *sidA* was used as the target gene. See Appendix A.4 for a list of primers. Real time qRT-PCR was carried out in 25 μL reaction volumes on a BIO-RAD iQ^{TM}5 Multicolor Real-Time PCR Detection System machine. The real time qRT-PCR consisted of the following a 3-step protocol: (95°C denaturation for 10 s, 55°C annealing period for 30 s, 72°C extension for 45 s) $\times$ 40 cycles. Cycling involved an initial denaturing / polymerase activation step (95°C for 3 min) and a final melting curve analysis (+0.5°C ramping $\times$ 81 cycles; 30 second incubation between each cycle). SYBR Green (Bioline) was used as the fluorescent reporter molecule in all reactions. Real time qRT-PCR mixes consisted of 2 μL template cDNA to 23 μL master mix: 12.5μL SYBR Green MM 2$\times$, 1μL forward primer at concentration 10μM/μL, 1μL reverse primer at concentration 10μM/μL, 8.5 1μL RNase-free water per one reaction. Relative gene expression (fold change from the addition of iron) was quantified using the Pfaffl method and normalized to β-tubulin [42]. Each experiment was performed in biological triplicate, and real time qRT-PCR was carried out in technical duplicates. Standard deviations were calculated to ensure statistical accuracy.

Chapter 7

Model Validation

The model prediction of genetic oscillations occurring in high iron environments was validated with new data not used in model construction. As all network genes are transcriptionally regulated by the transcription factors HapX and SreA, real time reverse transcriptase polymerase chain reaction (qRT-PCR) was used to quantify relative fold change in target gene expression. PCR is a method that allows exponential amplification of short DNA sequences. The amount of an expressed gene in a cell can be measured by the number of copies of that gene's mRNA transcript present in a sample. Hence to experimentally determine gene expression, I first extract RNA from lysed *A. fumigatus* cells, then convert the RNA to complementary DNA (cDNA), and finally use qRT-PCR to detect and amplify a specific targeted DNA sequence (our target gene) in the cDNA strand. Expression of the target gene, essentially the number of mRNA transcripts present in the cell at the time of sample collection, is normalized to a target gene control and also to a constitutively expressed house-keeping gene. Relative fold change is calculated using the well-accepted Pfaffl method and presented on a logarithmic scale [42].

Below, I show the experimental results for gene expression of *sidA*, the gene coding for enzyme SidA which catalyzes the first step in the biosynthesis of siderophores. Previous experimental results show that *sidA* gene expression is representative of gene expression in the entire iron acquisition system [1] [5] [10]. For the experiments, *A. fumigatus* was grown in iron depleted conditions for approximately 3.5 days. At this point the fungus was in a state of severe iron starvation. Subsequently iron was added to the media, and a time course was taken following this shift from iron depleted to iron replete conditions. Samples were collected at 0, 10, 60, 120, 240, 300, 330, 360, 390, 420, 450, 480, 510, 540, and 570 minutes after the addition of iron. It is necessary to collect samples frequently in order to observe oscillatory behavior. The experimental results in Figure 7.1 show evidence of oscillations in *sidA* gene expression. Also in Figure 7.1 is an SDDS model simulation fitted to data by adjusting propensity parameters slightly from the uniform random distribution. The simulation is an average of 100 SidA trajectories with propensity parameters listed in Table 7.1.

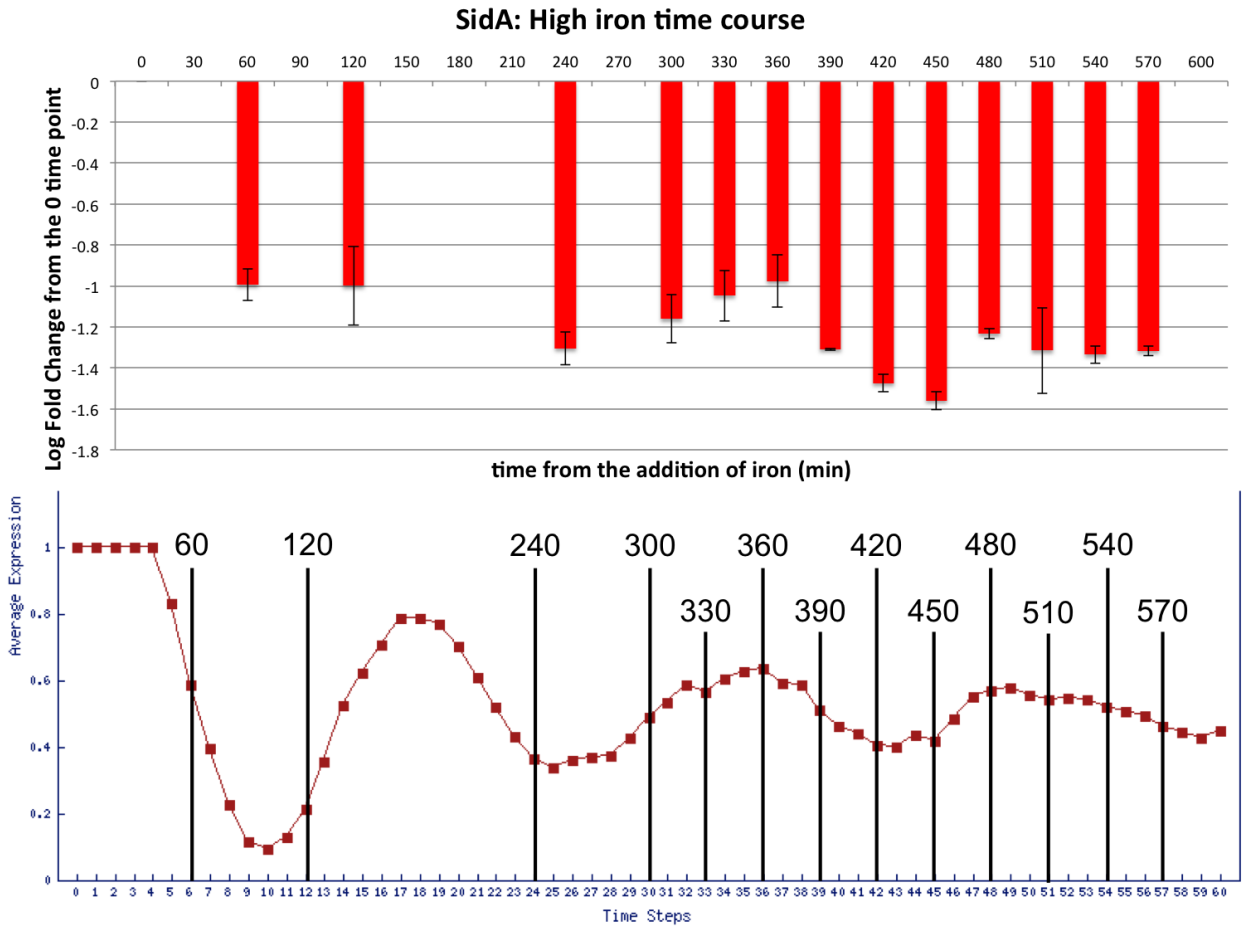

Figure 7.1: qRT-PCR results for SidA gene expression compared to an average of 100 stochastic simulations with propensity parameters listed in Table 7.1. Experimental data correlates well with SDDS model output if we consider 1 time step equal to 10 minutes.

Variable	$p^{\uparrow}$	$p^{\downarrow}$
Iron	1	1
HapX	.9	.6
SreA	.9	.6
SidA	.6	.6
RIA	.6	.6
TAFC	.6	.6
MirB	.6	.6
EstB	.4	.6
FC	.6	.6
VAC	.6	.5
ICP	.6	.6

Table 7.1: Propensity parameters for an SDDS model fitted to experimental results.

The propensity parameters were chosen for the following reasons:

- HapX and SreA are post-translationally regulated by iron whereas all other regulation occurs at the transcriptional level through transcription factors HapX and SreA. Therefore, activation of HapX and SreA happens very quickly (high $p^{\uparrow}$) as opposed to the comparatively slower transcriptional regulations.
- EstB has a low activation propensity to account for the fact that once TAFC is synthesized there is likely significant delay before it is secreted from the cell, sequesters iron from somewhere in the environment and is taken up again by the cell. Hence I assume that the update of EstB depends on TAFC synthesized in some previous generation.
- I also assume that levels of iron stored in the vacuole decrease somewhat more slowly than they increase.

Experimental gene expression data collected in a previous experiment for both *sidA* and *sreA* show similar oscillation patterns and are included in Appendix A.4, Figure A.2.

Chapter 8

Discussion

Aspergillus fumigatus is a ubiquitous, saprophytic fungus which has become an increasingly dangerous fungal pathogen of humans worldwide. Humans typically inhale hundreds of airborne *Aspergillus* spores a day [32]. In human hosts with normal, healthy immune systems *A. fumigatus* spores are easily cleared by host defense mechanisms. However in immunocompromised individuals *A. fumigatus* is responsible for invasive aspergillosis, a serious health risk with high mortality rates. At the forefront in the war fought between host immune response and invasive fungi is the battle for iron. During mammalian infection the host seeks to deprive the fungus of iron in part by binding free iron to host proteins such as transferrin while the fungus plots to steal host iron via siderophore-mediated iron sequestration. Often times the victor of this battle will determine whether infection persists. Notably, iron was shown to be essential for *A fumigatus* virulence in a mouse model of invasive aspergillosis [10] [11]. Furthermore, proteins in the iron regulatory network are thought to be promising drug targets owing to molecular differences in iron-handling between fungi and other eukaryotes [2]. Therefore, a more complete understanding of iron homeostasis in fungi is key to developing better drugs for treatment of invasive fungal infections. With this goal in mind, I constructed a dynamic mathematical model of iron acquisition, storage, and utilization in the fungus *Aspergillus fumigatus*. I chose to use discrete modeling frameworks as opposed to an ODE model for the following reasons:

- Very little quantitative information about fungal iron regulation such as kinetic parameters is known, and discrete models are built from qualitative information easily extracted from the literature.
- Discrete models are intuitive and more readily understood by a non-mathematical audience.
- Even while requiring less upfront information than ODE models, discrete models can accurately represent biological systems and provide new insights into underlying mechanisms.

Analysis of the deterministic discrete model shows that the model agrees with current literature except in the prediction of oscillations in gene expression in iron replete environments. This oscillatory behavior was further analyzed in a stochastic discrete framework for both single cell and multi-cell populations. In single cell stochastic simulations with a uniform randomly distributed update schedule, oscillations were preserved and sustained. For stochastic simulations with a uniform randomly distributed update schedule in a population of 100 cells, oscillations were sustained but damped over time. Oscillations in gene expression in a sustained high iron environment was validated by *in vitro* experiments using quantitative real-time RT-PCR.

It has been shown that spontaneous oscillations occur only in nonlinear dynamic open systems [27]. Biological systems are in general nonlinear dynamic open systems and thus are capable of exhibiting periodicity. In the model presented here interactions among network variables are certainly nonlinear (as can be seen in the PDS representation), and the external parameter, Iron, allows the network to continuously interact with its environment. Several studies using delay differential equation models report that time delays coupled with negative feedback motifs can give rise to oscillations [36] [43] [44]. Genetic oscillations play an important role in many dynamic cellular processes such as cell cycle and circadian clocks [28] [29]. Kruse *et al.* remark that genetic oscillations are commonly generated by negative feedback involving a transcription factor due to the time delay in producing mRNA, translating that mRNA into protein, and finally repression of the promoter region by the transcription factor [26]. Recently, damped oscillations in expression of genes involved in iron homeostasis in a single *E. coli* cell in a switch from an iron replete to an iron depleted environment were discovered using single-cell experiments and modeled using differential equations [36].

Similarly, I hypothesize that the sinusoidal oscillations in the *A. fumigatus* iron regulatory network derive from the mutual transcriptional control by the two transcription factors HapX and SreA, the double negative feedback between them, and time delays between transcription of the transcription factors and their actions as regulatory proteins on other genes in the system. Figure 8.1 demonstrates the time delay and negative feedback inherent in the transcriptional control. Recall that the model predicts significant oscillations a population of cells under high iron conditions. However, the model predicts very weak, damped oscillations even in a single cell under low iron conditions. This distinction may be explained by the fact that a switch from an iron depleted to an iron replete environment causes an initial spike in intracellular iron whereas a switch from an iron replete to an iron depleted environment does not. Amir *et al.* conclude that the oscillations they found in *E. coli* iron homeostasis were driven by intracellular iron oscillations resulting from a compromise between stability and speed of response [36]. Amir *et al.* explains that this compromise is likely necessary because iron is such a scare yet vital resource that cells have evolved methods of rapid iron uptake to exploit small windows of iron availability. Based on this reasoning, it seems logical to conclude that in a switch from an iron depleted to an iron replete environment *A.fumigatus* compromises between a greedy, rapid uptake of iron and the possibility of accumulating toxic amounts of iron by initially acquiring overly sufficient amounts of iron and subsequently cycling between intervals of iron uptake and iron usage. An additional contribution to oscillations may be due to the fact that HapX and SreA are regulated post-translationally by iron; however when present they inhibit the other's transcription. Therefore the response of regulatory proteins to iron is fast whereas the inhibitory effect on each is comparatively slow. This potentially contributes to oscillations by causing iron levels to continually overshoot and undershoot ideal levels.

In summary, oscillations in the iron regulatory network in iron replete environments may be instigated by fluctuations in intracellular iron. As extracellular iron is fixed at high, these fluctuations in intracellular iron alone determine which transcription factor, HapX or SreA, is inhibited and which is activated. Finally I expect that the mutual transcriptional control by HapX and SreA, the double negative feedback between them, and the time lag from the start of transcription to the end of translation propagates and maintains oscillations in the entire iron regulatory network.

Kurse and Jlicher state that "The emergence of oscillations in a complex system is subtle...Therefore, theoretical approaches are an essential tool in the study of cellular oscillations" [26]. Oscillations can be difficult to observe experimentally if one is not already looking for them. For instance, in order to observe oscillations in the *A. fumigatus* iron regularity network, it was necessary to take

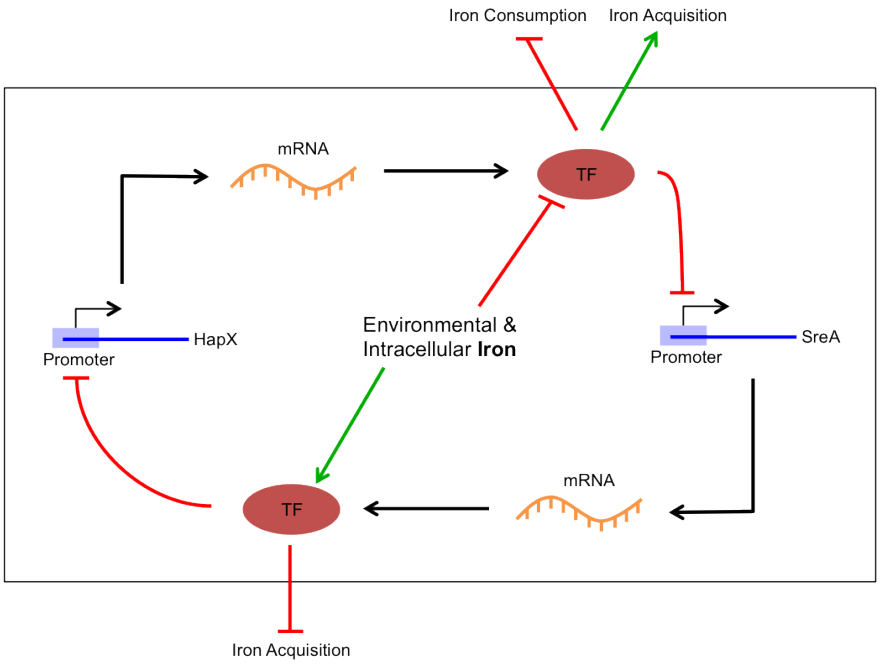

Figure 8.1: Mutual transcriptional control by HapX and SreA. HapX and SreA are modified in response to iron post translationally. Other network genes are regulated by HapX and SreA at the transcriptional level.

very frequent time points over a long time course. This research showcases the predictive power of mathematical modeling.

Bibliography

[1] Schrettl, M., Kim, H. S. Eisendle, M., Kragl, C., Nierman, W. C., Heinekamp, T., Werner, E. R., Jacobsen, I., Illmer, P., Yi, H., Brakhage, A. A., Haas, H., **SreA-mediated iron regulation is Aspergillus fumigatus**. *Molecular microbiology* 2008, **70**: 27-43.

[2] Haas, H., **Iron - A Key Nexus in the Virulence of Aspergillus fumigatus**. *Frontiers in microbiology* 2012, **3**: 28.

[3] Haas, H., **Iron homeostasis–Achilles' heel of Aspergillus fumigatus?** *Current opinion in microbiology* 2011, **14**: 400-405.

[4] Schrettl, M., Beckmann, N., Varga, J., Heinekamp, T., Jacobsen, I. D., Jochl, C., Moussa, T. A., Wang, S., Gsaller, F., Blatzer, M., Werner, E. R., Niermann, W. C., Brakhage, A. A., Haas, H., **HapX-mediated adaption to iron starvation is crucial for virulence of Aspergillus fumigatus**. *PLoS pathogens* 2012, 6: 1001-1124.

[5] Tracy Power, Montserrat Ortoneda, John P. Morrissey, Alan D. W. Dobson, **Differential expression of genes involved in iron metabolism in Aspergillus fumigatus**. *International Microbiology* 2006, **9**: 281-287.

[6] Schrettl, M., Bignell, E., Kragl, C., Sabiha, Y., Loss, O., Eisendle, M., Wallner, A., Arst, H. N., Haynes, K., Haas, H., **Distinct Roles for Intra- and Extracellular Siderophores during Aspergillus fumigatus Infection**. *PLoS Pathogens* 2007, **3**: (9) 1195-1207.

[7] Kragl, C., Schrettl, M., Abt, B., Sarg, B., Lindner, H. H., Haas, H., **EstB-mediated hydrolysis of the siderophore triacetylfusarinine C optimizes iron uptake of Aspergillus fumigatus**. *Eukaryotic cell* 2007, **6**: 1278-85.

[8] Wallner, A., Blatzer, M., Schrettl, M., Sarg, B., Lindner, H., Haas, H., **Ferricrocin, a siderophore involved in intra- and transcellular iron distribution in Aspergillus fumigatus**. *Applied and environmental microbiology* 2009, **75**: 4194-6

[9] Eisendle, M., M. Schrettl, C. Kragl, D. Muller, P. Illmer, and H. Haas. **The intracellular siderophore ferricrocin is involved in iron storage, oxidative stress resistance, germination, and sexual development in Aspergillus nidulans**. *Eukaryotic Cell* 2006, **5**:15961603.

[10] Schrettl M., Bignell E., Kragl C., Joechl C., Rogers T., N. Arst Jr. H., Haas H., **Siderophore biosynthesis but not reductive iron assimilation is essential for Aspergillus fumigatus virulence**. *J. Exp. Med.* 2004,**200**: 1213-1219.

[11] Hissen, A. H. T., Wan, A. N. C., Warwas, M. L., Pinto, L. J., Moore, M. M., **The Aspergillus fumigatus Siderophore Biosynthetic Gene sidA, Encoding L-Ornithine N^5-Oxygenase, Is Required for Virulence**. *Infection and Immunity* 2005, **73**: 5493-5503.

[12] Zarember KA, Sugui JA, Chang YC, Kwon-Chung KJ, Gallin JI, **Human polymorphonuclear leukocytes inhibit Aspergillus fumigatus conidial growth by lactoferrin-mediated iron depletion**. *J Immunol* 2007, **178**:6367-6373.

[13] Haas, H., Eisendle, M., and Turgeon, B. G., **Siderophores in fungal physiology and virulence**. *Annual Reviews -Phytopathology* 2008, **46**: 149187.

[14] Blatzer, M., Barker, B. M., Willger, S. D., Beckmann,N., Blosser, S. J., Cornish, E. J., Mazurie, A., Grahl, N., Haas,H., Cramer, R. A., **SREBP coordinates iron and ergosterol homeostasis to mediate triazole drug and hypoxia responses in the human fungal pathogen *Aspergillus fumigatus***. *PLoS Genetics* 2011, **7**: e1002374. doi:10.1371/journal.pgen.1002374.

[15] Linde, J., Hortschansky, P., Fazius, E., Brakhage, A., Guthke, R., Haas, H., **Regulatory interactionis for iron homoeostatis in Aspergillus fumigatus inferred by a Systems Biology approach**. *BMC Systems Biology* 2012, **6**: 6, doi:10.1186/1752-0509-6-6.

[16] Blatzer, M., Binder, U., and Haas, H., **The metalloreductase FreB is involved in adaptation of Aspergillus fumigatus to iron starvation**. *Fungal Genetics and Biology* 2011, **48**: 10271033.

[17] Nilius, AM., Farmer SG., **Identification of extracellular siderophores of pathogenic strains of Aspergillus fumigatus**. *Journal of medical and veterinary mycology* 1990, **28**(5): 395-403.

[18] Hissen, A. H. T., Chow, J. M. T., Pinto, L. J., Moore, M. M., **Survival of Aspergillus fumigatus in Serum Involves Removal of Iron from Transferrin: the Role of Siderophores**. *Infection and Immunity* 2004, 72: 1402-1408.

[19] Gsaller, F., Eisendle, M., Lechner, B. E., Schrettl, M., Lindner, H., Muller, D., Geley, S., Haas, H., **The interplay between vacuolar and siderophore-mediated iron storage in Aspergillus fumigatus** *Metallomics* 2012, **4**: 1262-1270.

[20] Hortschansky P., Eisendle M., Al-Abdallah Q., Schmidt A. D., Bergmann S., Thon M., Kniemeyer O., Abt B., Seeber B., Werner E. R. et al, **Interaction of HapX with the CCAAT-binding complex-a novel mechanism of gene regulation by iron**. *EMBO Journal* 2007, **26**: 3157-3168.

[21] Nierman, W. C. *et. al.*, **Genomic sequence of the pathogenic and allergenic filamentous fungus *Aspergillus fumigatus***. *Nature* 2005, **438**: 22-29.

[22] Veliz-Cuba A., Salam Jarrah A., Laubenbacher R., **Polynomial Algebra of Discrete Models in Systems Biology**. *Bioinformatics* 2010, **26** (13): 1637-1643.

[23] R. Lidl, H. Niederreiter. *Finite Fields.* Cambridge University Press, New York, 1997.

[24] Laubenbacher, R., Stigler, B. **A computational algebra approach to the reverse engineering of gene regulatory networks.** *Journal of Theoretical Biology* 2004, **299**: 523-537

[25] Hinkelmann, F., Brandon, M., Guang, B., McNeill, R., Blekherman, G., Veliz-Cuba, A., Laubenbacher, R. ADAM: Analysis of Discrete Models of Biological Systems Using Computer Algebra. *BMC Bioinformatics* 2011, DOI: 10.1186/1471-2105-12-295http://dx.doi.org/10.1186/1471-2105-12-295

[26] Kruse, K., Jlicher, F., **Oscillations in cell biology**. *Current Opinion in Cell Biology* 2005, **17**: 20-26

[27] Strogatz, S. H. *Nonlinear Dynamics and Chaos: With Applications to Physics, Biology, Chemistry, and Engineering.* Reading, Mass: Addison-Wesley,1994.

[28] Tyson, J. J., Chen, K., Novak, B., **Network dynamics and cell physiology**. *Nature Reviews Molecular Cell Biology* 2001, **2**: 908-916.

[29] Dunlap, J. C. **Molecular bases for circadian clocks** *Cell* 1999, **96**: 271-290.

[30] Murrugarra, D., Veliz-Cuba, A., Aguilar, B., Arat, S., Laubenbacher, R., **Modeling stochasticity and variability in gene regulatory networks** *EURASIP Journal on Bioinformatics and Systems Biology* 2012, **2012** (1): 5.

[31] Palsson, B., *SystremsBiology:SimulationofDynamicNetworkStates.* CambridgeUniversity Press, 2011

[32] Lass-Florl, C., Roilides, E., Loffler, J., Wilflingseder, D., Romani, L., **Minireview: host defence in invasive aspergillosis**. *Mycoses* 2013, doi:10.1111/myc.12052.

[33] Lin, S., Schranz, J., Teutsch, S.M., **Aspergillosis Case-Fatality Rate: Systematic Review of the Literature**. *Clinical Infectious Diseases* 2001, 32: 358-66

[34] Steinbach, W., Marr, K., Anaissie, E., Azie, N., Quan, S., Meier-Kriesche, H., Apewokin, S., Horn, D., **Clinical epidemiology of 960 patients with invasive aspergillosis from the PATH Alliance registry**. *British Infection Association* 2012, **65**: 453-64.

[35] Hsiang, T., Baillie, D. L. **Comparison of the yeast proteome to other fungal genomes to find core fungal genes**. *J. Mol. Evol.* 2005, **60**: 475483.

[36] Amir, A., Meshner, S., Beatus, T., Stavans, J., **Damped oscillations in the adaptive response of the iron homeostasis network of E. coli**. *Molecular Microbiology* 2010, **76**(2): 428-436.

[37] Weinber, E., **Iron availability and infection** *Biochimica et Biophysica Acta* 2008, **1790**: 600-605.

[38] Elowitz, M. B., Levine, A. J., Siggia, E. D., Swain, P. S., **Stochastic Gene Expression in a Single Cell**. *Science* 2002, **297** (5584): 1183-1186.

[39] Swain, P.S., Elowitz, M. B., Siggia, E. D., **Intrinsic and extrinsic contributions to stochasticity in gene expression**. *PNAS* 2002, **99** (20): 12795-800.

[40] Ozbudak, E. M., Thattai, M., Kurtser, I., Grossman, A. D., van Oudenaarden, A., **Regulation of noise in the expression of a single gene**. *Nature Genetics* 2002, **31**(1): 69-73.

[41] Ko, M. S., **Induction mechanism of a single gene molecule: stochastic or deterministic?** *Bioessays* 1992, **14**(5): 341-6.

[42] Pfaffl, M. W., **A new mathematical model for relative quantification in real-time RT-PCR**. *Nucleic Acids Research* 2001, **29**(9):e45.

[43] Maithreye, R., Sarkar, R.R., Parnaik, V.K., Sinha, S., **Delay-induced transient increase and heterogeneity in gene expression in negatively auto-regulated gene circuits**. *PloS One* 2008, **3**(8):e2972.

[44] Mahaffy, J. M., Pao, C. V., **Models of genetic control by repression with time delays and spatial effects**. *Journal of Mathematical Biology* 1984, **20**(1): 39-57.

Appendix A

Appendix

A.1 Transition Tables

Iron(t)	Iron(t+1)
0	0
1	1

Table A.1: Transition table for extracellular iron.

Iron(t)	VAC(t)	SreA(t)	HapX(t+1)
0	0	0	1
0	0	1	0
0	1	0	1
0	1	1	0
0	2	0	1
0	2	1	0
1	0	0	1
1	0	1	0
1	1	0	1
1	1	1	0
1	2	0	0
1	2	1	0

Table A.2: Transition table for HapX.

Iron(t)	VAC(t)	HapX(t)	SreA(t+1)
0	0	0	0
0	0	1	0
0	1	0	0
0	1	1	0
0	2	0	0
0	2	1	0
1	0	0	0
1	0	1	0
1	1	0	0
1	1	1	0
1	2	0	1
1	2	1	0

Table A.3: Transition table for SreA.

SreA(t)	HapX(t)	SidA(t+1)
0	0	0
0	1	1
1	0	0
1	1	0

Table A.4: Transition table for SidA.

Iron(t)	HapX(t)	SreA(t)	RIA(t+1)
0	0	0	0
0	0	1	0
0	1	0	0
0	1	1	0
1	0	0	0
1	0	1	0
1	1	0	1
1	1	1	0

Table A.5: Transition table for RIA.

Iron(t)	HapX(t)	SreA(t)	RIA(t+1)
0	0	0	0
0	0	1	0
0	1	0	1
0	1	1	0
1	0	0	1
1	0	1	1
1	1	0	1
1	1	1	1

Table A.6: Transition table for TAFC.

SreA(t)	HapX(t)	MirB(t+1)
0	0	0
0	1	1
1	0	0
1	1	0

Table A.7: Transition table for MirB.

Iron(t)	MirB(t)	TAFC(t)	EstB(t+1)
0	0	0	0
0	0	1	0
0	1	0	0
0	1	1	1
1	0	0	0
1	0	1	0
1	1	0	0
1	1	1	2

Table A.8: Transition table for EstB.

EstB(t)	SidA(t)	FC(t)	FC(t+1)
0	0	0	0
0	0	1	1
0	0	2	1
0	1	0	1
0	1	1	1
0	1	2	1
1	0	0	0
1	0	1	1
1	0	2	1
1	1	0	1
1	1	1	1
1	1	2	1
2	0	0	0
2	0	1	2
2	0	2	2
2	1	0	1
2	1	1	2
2	1	2	2

Table A.9: Transition table for FC.

EstB(t)	RIA(t)	VAC(t)	VAC(t+1)
0	0	0	0
0	0	1	0
0	0	2	1
0	1	0	1
0	1	1	1
0	1	2	1
1	0	0	1
1	0	1	1
1	0	2	1
1	1	0	1
1	1	1	2
1	1	2	2
2	0	0	1
2	0	1	2
2	0	2	2
2	1	0	2
2	1	1	2
2	1	2	2

Table A.10: Transition table for VAC.

FC(t)	VAC(t)	HapX(t)	ICP(t+1)
0	0	0	0
0	0	1	0
0	1	0	2
0	1	1	1
0	2	0	2
0	2	1	1
1	0	0	0
1	0	1	0
1	1	0	2
1	1	1	1
1	2	0	2
1	2	1	1
2	0	0	1
2	0	1	1
2	1	0	2
2	1	1	1
2	2	0	2
2	2	1	1

Table A.11: Transition table for ICP.

A.2 Polynomial Dynamical System

x_1 = external iron
x_2 = HapX
x_3 = SreA
x_4 = SidA
x_5 = RIA
x_6 = TAFC
x_7 = MirB
x_8 = EstB
x_9 = FC
x_{10} = VAC
x_{11} = ICP

$f_1 = x_1$

$f_2 = x_1^2x_{10}^2x_3^2 - x_1^2x_{10}x_3^2 + x_1x_{10}^2x_3^2 - x_1^2x_{10}^2 - x_1^2x_3^2 - x_1x_{10}x_3^2 + x_1^2x_{10} - x_1x_{10}^2 + x_1x_3^2 + x_1^2 + x_1x_{10} - x_3^2 - x_1 + 1$

$f_3 = -x_1^2x_{10}^2x_2^2 + x_1^2x_{10}x_2^2 - x_1x_{10}^2x_2^2 + x_1^2x_{10}^2 + x_1x_{10}x_2^2 - x_1^2x_{10} + x_1x_{10}^2 - x_1x_{10}$

$f_4 = x_3^2x_2^2 + x_3^2x_2 - x_2^2 - x_2$

$f_5 = -x_1^2x_2^2x_3^2 - x_1^2x_2x_3^2 - x_1x_2^2x_3^2 + x_1^2x_2^2 - x_1x_2x_3^2 + x_1^2x_2 + x_1x_2^2 + x_1x_2$

$f_6 = x_4^2x_6^2x_7^2 + x_4^2x_6^2x_7 - x_4x_6^2x_7^2 - x_4^2x_6x_7 + x_4x_6^2x_7 - x_4^2x_7^2 + x_4x_6x_7^2 + x_6^2x_7^2 - x_4^2x_6 - x_4x_6^2 + x_4^2x_7 - x_4x_6x_7 - x_4x_7^2 + x_6x_7^2 - x_4^2 + x_4x_6 - x_6^2 + x_4x_7 - x_4 - x_6$

$f_7 = x_3^2x_2^2 + x_3^2x_2 - x_2^2 - x_2$

$f_8 = x_1x_7^2x_6^2 + x_1x_7^2x_6 + x_1x_7x_6^2 + x_7^2x_6^2 + x_1x_7x_6 + x_7^2x_6 + x_7x_6^2 + x_7x_6$

$f_9 = -x_8^2x_4^2x_9^2 + x_8^2x_4x_9^2 + x_8x_4^2x_9^2 - x_8^2x_9^2 - x_8x_4x_9^2 - x_4^2x_9^2 + x_8x_9^2 - x_4^2 + x_9^2 - x_4$

$f_{10} = x_8^2x_5^2x_10^2 + x_8^2x_5^2x_{10} + x_8^2x_5x_{10}^2 + x_8x_5x_{10}^2 + x_5^2x_{10}^2 + x_8^2x_5 - x_8x_5^2 - x_8^2x_{10} - x_5^2x_{10} + x_8x_{10}^2 + x_8^2 - x_8x_5 - x_5^2 - x_{10}^2 - x_5 + x_{10}$

$f_{11} = x_9^2x_{10}^2x_2^2 - x_9^2x_{10}^2x_2 - x_9x_{10}^2x_2^2 + x_9^2x_{10}^2 + x_9x_{10}^2x_2 - x_9^2x_2^2 - x_9x_{10}^2 + x_9^2x_2 - x_{10}^2x_2 + x_9x_2^2 - x_9^2 - x_{10}^2 - x_9x_2 + x_9$

A.3 Supplementary Figures

A.4 Supplementary Experimental Information

The **Pfaffl** method was used to quantify fold change from real-time qRT-PCR results [42]:

Let E_t and E_r be the efficiency of the target gene and reference gene respectively. Define $\Delta_t = C_t$ value of target gene control $-C_t$ value of target gene treated. Define $\Delta_r = C_t$ value of reference gene control $-C_t$ value of reference gene treated. Then:

fold change in target gene expression = $E_t^{\Delta_t}$,
fold change in reference gene expression = $E_r^{\Delta_r}$ and
ratio target gene expression = fold change in target gene / fold change in reference gene = $\frac{E_t^{\Delta_t}}{E_r^{\Delta_r}}$.

It was assumed that $E_t = 1.936$ and $E_r = 1.943$. C_t values were averaged across technical duplicates. Standard deviations were calculated based on biological triplicates.

Gene		Primer Sequence (5'-3')	melting Tm (°C)	Product size(bp)
β-tubuliln	FP	CTGCTCTGCCATTTTCCGTG	56.8	119
	RP	CGGTCTGGATGTTGTTGGGA	57.3	
sidA	FP	TGACGACTCGCCTTTTGTGAA	57.0	474
	RP	TTGCTCGGGTCCATCTCAAC	57.3	
sreA	FP	CTCAGTACGATCGCTTCCCC	57.3	297
	RP	GTCCCACAATTACTGCACGA	55.2	
hapX	FP	CCCATCAGCCAGGCTACAAA	57.5	274
	RP	AGGCGTCGGCACAAGATAAA	57.0	
ftrA	FP	GGCATGATCGGAGCGTTCTA	57.1	411
	RP	GGCTTGGTTTCCTCCTCGAT	57.2	
cccA	FP	GAGCCAAGAGTGAGGCAGAA	57.0	448
	RP	TGCACACCACCCTTGATACC	57.4	
cat1	FP	GACACTCAGCTGAACCGTCA	57.1	109
	RP	TGAACATTTGGCCTGCTCCA	57.4	
mirB	FP	GGGTTCGGTGGGCTTTCATA	57.5	346
	RP	GAAGAACTCCGGGCAGATCA	56.8	

Table A.12: Primers used for real-time qRT-PCR.

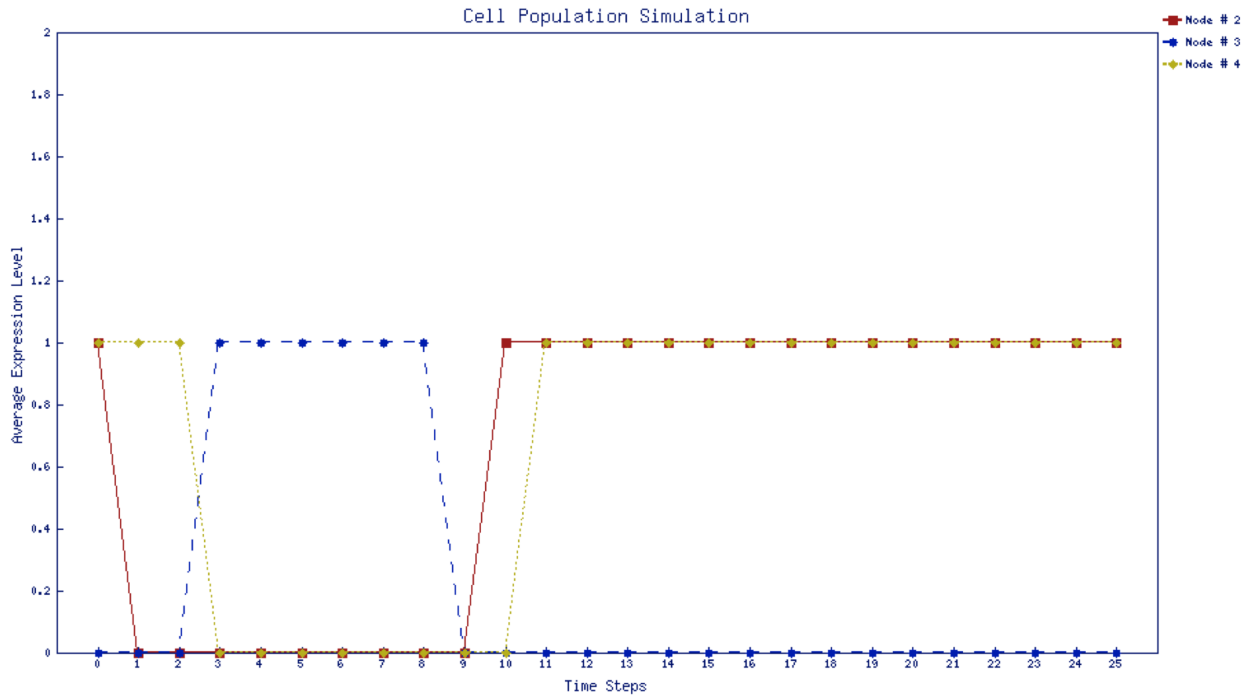

(a) Sample stochastic trajectory under uniform random update distribution of node1=HapX, node2=SreA, node3=SidA in a single cell population. Oscillations are weak and dampen quickly. The model is initialized from a point of high intracellular and extracellular iron.

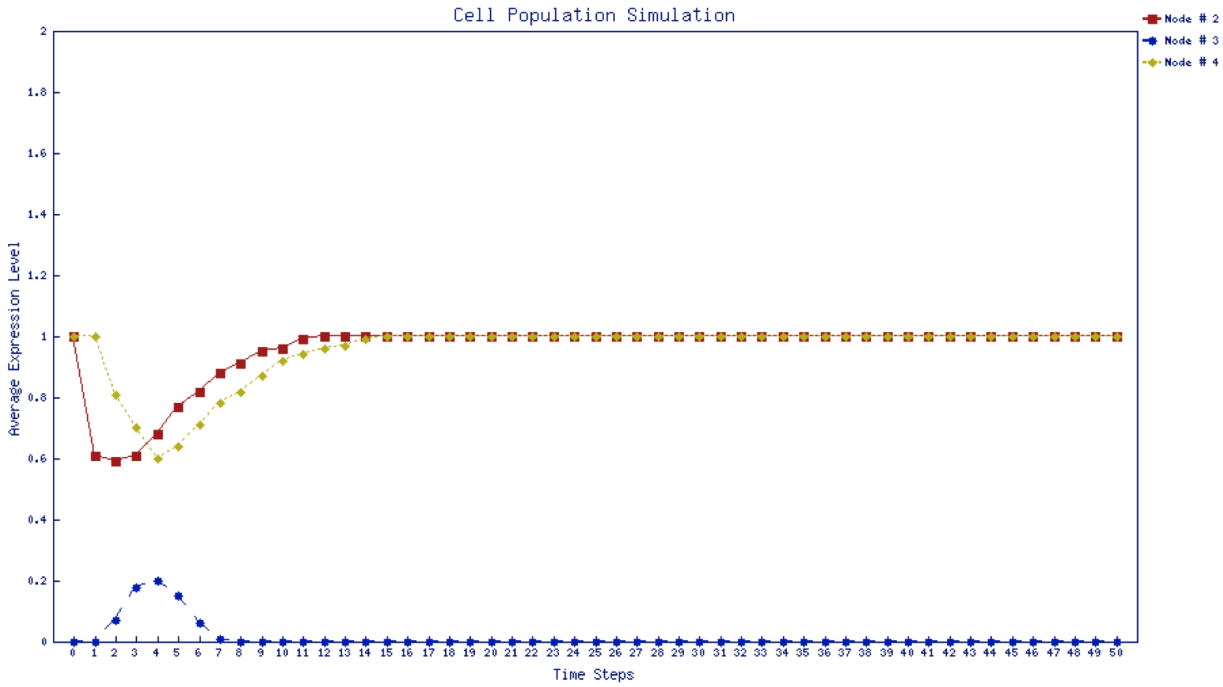

(b) Sample stochastic trajectory under uniform random update distribution of node1=HapX, node2=SreA, node3=SidA in a 100 cell population. Oscillations are weak and dampen quickly. The model is initialized from a point of high intracellular and extracellular iron.

Figure A.1: Stochastic trajectories with a uniform random distribution of update schedules in a switch from high to low iron environment.

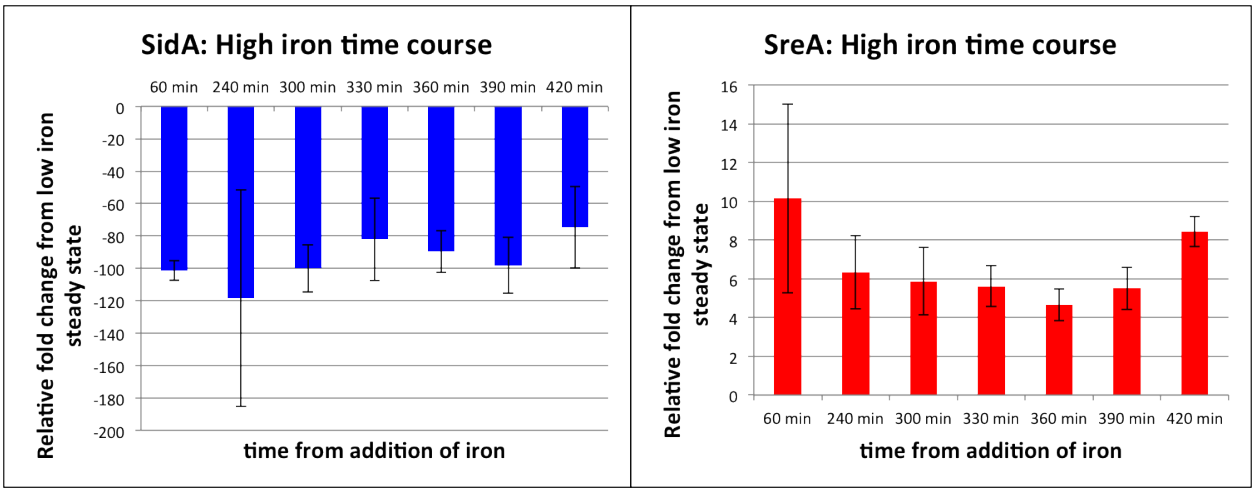

Figure A.2: qRT-PCR gene expression results from a preliminary experiment for *sidA* and *sreA*.

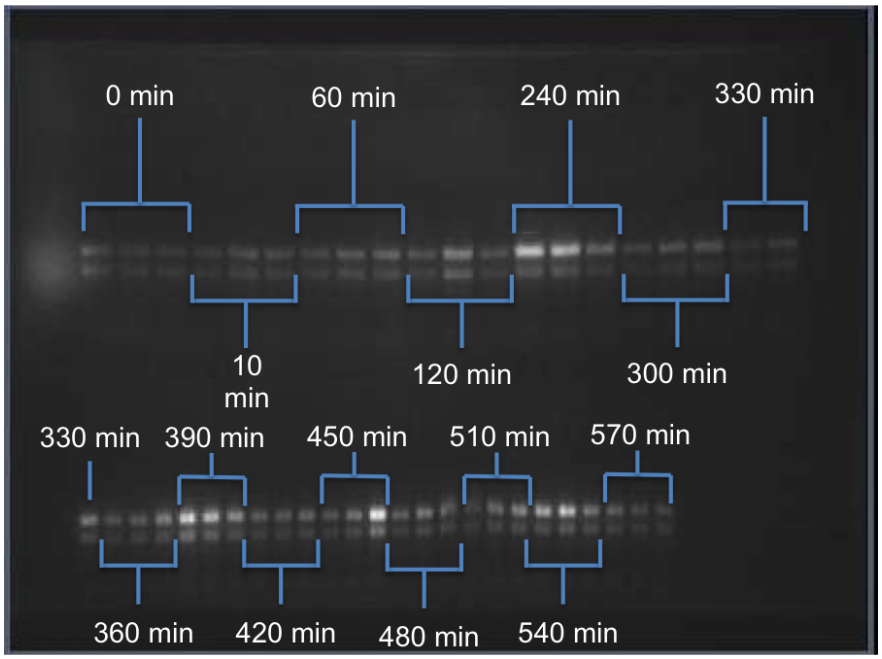

Figure A.3: Gel electrophoresis results from RNA quality check for the experiment in Figure 7.1. No RNA samples were degraded.

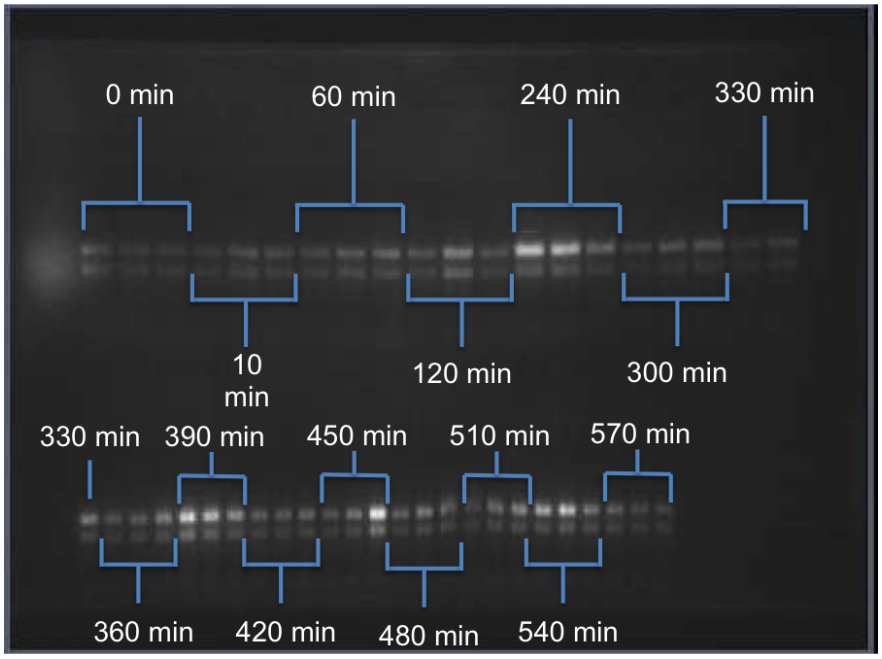

Figure A.4: Gel electrophoresis results from RNA quality check for the experiment in Figure A.2. Three RNA samples from different sets of triplicates were degraded and were not used in qRT-PCR.